
Electronic Thesis and Dissertation Repository

4-29-2016 12:00 AM

Polymer System and Molding Techniques for Surgical Training Models

Daniel J. Park
The University of Western Ontario

Supervisor
Dr. Andrew N. Hrymak
The University of Western Ontario

Graduate Program in Chemical and Biochemical Engineering
A thesis submitted in partial fulfillment of the requirements for the degree in Master of Engineering Science
© Daniel J. Park 2016

Follow this and additional works at: <https://ir.lib.uwo.ca/etd>

 Part of the [Polymer Science Commons](#)

Recommended Citation

Park, Daniel J., "Polymer System and Molding Techniques for Surgical Training Models" (2016). *Electronic Thesis and Dissertation Repository*. 3747.
<https://ir.lib.uwo.ca/etd/3747>

This Dissertation/Thesis is brought to you for free and open access by Scholarship@Western. It has been accepted for inclusion in Electronic Thesis and Dissertation Repository by an authorized administrator of Scholarship@Western. For more information, please contact wlsadmin@uwo.ca.

Abstract

Poly(vinyl alcohol) (PVA) hydrogels are used to produce high fidelity models for surgical training applications. PVA hydrogel mechanical properties are developed through the use of a freeze-thaw cycling, physical crosslinking process. The resulting gels exhibit a non-linear elastic modulus which can be tailored to match many tissues of the human body.

Methods for joining PVA hydrogels were investigated to aid in the production of complicated structures that would be difficult to produce in a single step. Bond strength of PVA gels was characterized using a modified peel test. The porosity and degree of crosslinking of the PVA substrate were investigated as the factors affecting adhesion.

Rotational molding was investigated to produce hollow structures unattainable by injection molding. Fumed silica was used as a rheology modifier to maintain a molded shape before freeze-thaw cycling at room temperature. A prototype stomach and embedded vessel model were produced using the rotational molding and joining methods respectively.

KEYWORDS: Poly(vinyl alcohol), PVA, hydrogels, surgical training, adhesion and rotational molding

Acknowledgments

I would like to thank my supervisor, Dr. Andrew N. Hrymak for his guidance and support throughout my internship and graduate studies.

I would like to thank my advisor Dr. Leonardo E. Millon, from LifeLike BioTissue, for supporting me both academically and as a close friend. I had the pleasure of working with Dr. Millon and Spencer Lauzon of LifeLike over the past five years in research and development.

I would like to acknowledge Nazanin Afghan, Ines Griffoux and Lucas Ziliani for their work in the lab supporting this research.

Finally, I would like to thank my family and my spouse, Natasha MacDonald, for the support and patience throughout my studies.

Table of Contents

Abstract.....	ii
Acknowledgments.....	iii
Table of Contents.....	iv
List of Figures.....	vii
List of Tables.....	ix
Chapter 1.....	1
1 Introduction.....	1
1.1 Motivation.....	1
1.2 Objectives.....	2
1.3 Outline.....	2
Chapter 2.....	3
2 Literature Review.....	3
2.1 Introduction.....	3
2.2 A Brief History of Surgical Training.....	3
2.3 Modern Surgical Training Simulation.....	4
2.4 Hydrogels.....	6
2.5 Poly(vinyl alcohol) hydrogels.....	7
2.6 Adhesion.....	10
2.7 Rotational Molding and Casting.....	11
2.8 Summary.....	11
Chapter 3.....	12
3 Experimental Methods – Joining.....	12
3.1 Introduction.....	12
3.2 Material Preparation.....	12
3.2.1 Poly(vinyl alcohol) solution preparation.....	12
3.3 Uniaxial Tensile Testing.....	13
3.3.1 Sample Preparation.....	13
3.3.2 Equipment.....	16
3.3.3 Uniaxial Tensile Test.....	19
3.4 Peel Strength.....	20
3.4.1 ASTM D903-98 Peel Strength Standard.....	20

3.4.2	Sample Preparation	21
3.4.3	Testing.....	25
3.5	DSC.....	26
3.5.1	Introduction.....	26
3.5.2	Equipment.....	26
3.5.3	Sample Preparation	26
3.5.4	Testing.....	27
3.6	Dissolution of PVA hydrogel.....	28
3.6.1	Introduction.....	28
3.6.2	Sample Preparation	28
3.6.3	Testing.....	29
Chapter 4	30
4	Experimental Methods – Rotational Molding.....	30
4.1	Introduction.....	30
4.2	Thickening Agent.....	30
4.3	Rotational Molding Machine	31
4.4	Mold Making	36
4.5	Material Preparation.....	40
4.6	Molding.....	41
Chapter 5	43
5	Data Analysis	43
5.1	Uniaxial Tensile Testing.....	43
5.1.1	Stress Strain	43
5.1.2	Curve Fitting.....	44
5.1.3	Polymer Fraction.....	46
5.1.4	Analysis of Variance (ANOVA).....	48
5.2	Differential Scanning Calorimetry.....	48
5.2.1	Crystallinity.....	48
5.2.2	Porosity	49
5.3	Peel Strength	51
5.4	Stability of PVA hydrogel	52
Chapter 6	53
6	Results and Discussion.....	53

6.1 Introduction.....	53
6.2 Uniaxial Tensile.....	53
6.2.1 Stress-Strain.....	53
6.2.2 Water Loss.....	56
6.3 Peel Strength.....	57
6.4 Crystallinity.....	58
6.5 Porosity.....	60
6.6 Stability of PVA hydrogel.....	62
6.7 Application of Controlled Adhesion.....	64
6.8 Rotational Molding.....	65
6.8.1 Thickener Effect on Elastic Modulus.....	67
6.8.2 Thickener Effect on Residual Stress.....	68
6.9 Summary.....	69
Chapter 7.....	72
7 Conclusions.....	72
Chapter 8.....	73
8 Future Applications and Outlook.....	73
8.1 Introduction.....	73
9 References.....	75
Appendices.....	83
Appendix A: Ring Extensometry.....	83
Appendix B: Tensile Fixture Drawings.....	84
Appendix C: ASCII command table for ESM301L test stand.....	88
Curriculum Vitae.....	89

List of Figures

Figure 1 - Chemical structure of poly(vinyl alcohol)	7
Figure 2 – Diagram of PVA injection sheet mold. Not shown is the steel binding clamps used for mold closure.	13
Figure 3 – Rotary cutting of tensile samples	15
Figure 4 – Trapezoidal rebound of punch cutting samples.....	16
Figure 5 – Grip alignment fixture	17
Figure 6 – Tensile soft tissue grips with 10x50x2.2mm sample.....	18
Figure 7 – User interface for tensile test stand	19
Figure 8 – ASTM D903 peel strength specimen	22
Figure 9 – Linen embedded in peel specimens before bonding to alignment plate.....	23
Figure 10 – Rotational Molding Machine.....	32
Figure 11 –Rotation axis of molding machine.....	33
Figure 12 – Trace of mold orientation for select gear ratios (outer:inner)	35
Figure 13 – CAD model of stomach demonstrator part.....	37
Figure 14 – FDM printed stomach positives in ABS plastic	38
Figure 15 – Centroform EZFORM model LV 1827 with stomach positive forms	39
Figure 16 – Stomach mold halves, 0.8mm HIPS	40
Figure 17 – Stomach mold clamped prior to rotomolding.....	42
Figure 18 – Uncorrected tensile response for 10 w/% PVA.....	54
Figure 19 - Tensile response for 10 w/% PVA corrected for water loss	55

Figure 20 – Typical DSC heating curve for freeze-thaw cycle n=6 PVA hydrogel59

Figure 21 - Free water volume fraction with dashed horizontal line representing the total water volume in the sample. 61

Figure 22 – PVA volume fraction comparison as-made and immersed in deionized water... 63

Figure 23 – Embedded vessel model (left) dissection of vein (right) cross section 64

Figure 24 – Stomach 5 PPH Fumed Silica 10 w% PVA, under filled (frozen)..... 65

Figure 25 – Stomach model 4.25PPH fumed silica, 10w% PVA. (left) Stomach as made (right) stomach in expanded state. 66

Figure 26 – Modulus of fumed silica thickened PVA hydrogel normalized to control PVA without thickener addition. (Left) 3rd freeze-thaw cycle (right) 6th freeze-thaw cycle..... 67

Figure 27 – Typical normalized hysteresis curves for non-thickened and thickened PVA during first load-unload cycle in tension. (left) freeze-thaw cycle 3 (right) freeze-thaw cycle 6..... 69

List of Tables

Table 1 – Temperature Profile for a Single Freeze-Thaw Cycle	14
Table 2 – Summary of peel samples tested	24
Table 3 – Fumed silica thickener additional levels	41
Table 4 – PVA content hydrogels at various cycles for tensile correction	56
Table 5 – Peeling strength at various cycles, ASTM D903-98	57

Chapter 1

1 Introduction

1.1 Motivation

Surgical procedures require a great deal of knowledge and skill to be completed successfully. This is apparent due to the rigorous training surgeons undergo during their career. In Canada, after obtaining a medical degree, a surgery resident will complete between four and six years in a surgical residency program, with subspecialties potentially requiring more [1]. Residents will complete clinical rotations gaining exposure to and developing technical skills. At the same time they will also complete course work to develop a knowledge base [2].

The technical skills of a surgeon are always best gained through practice. A surgeon gains increased exposure throughout their residency, which will ultimately lead to independent practice [3]. Once competency at a particular task has been demonstrated, residents may be permitted to perform that task independently. A great deal of oversight is implemented due to its potential impact on human life. The public expects well trained surgeons and as such must accept that a large portion of learning is achieved in practice.

Other methods of practicing surgical techniques are common. Some examples include cadavers, animals, virtual reality and anatomical models. They each have a degree of fidelity to the human tissues and structure; however, none can completely replace real operating room exposure. Synthetic materials such as silicone rubber dominate the

available anatomical models; however, they lack the mechanical characteristics and tactile realism of human tissue.

An ideal candidate material for surgical models is one that displays the response and high water content of natural tissues. Polyvinyl Alcohol (PVA) hydrogels are ideal candidate materials. They exhibit a controllable non-linear stress-strain response similar to natural tissue. They also form stable gels in excess of 95% water.

1.2 Objectives

The objective of this work was to investigate methods for producing complex surgical training models. This work is divided into two research streams: joining methods for PVA gels and molding techniques to produce complex geometries. The final goal was to apply the understanding gained in both streams to produce surgical training models that were not otherwise possible with previous state of the art methods.

1.3 Outline

A review of literature relating to hydrogels, surgical training models, adhesion of gels and molding techniques is presented in chapter 2. Chapter 3 and 4 detail the equipment and experimental methods conducted in this research for joining and rotational molding respectively. Data analysis is presented in chapter 5. The results are presented and discussed in chapter 6. Chapters 7 and 8 presents the conclusions and future work respectively.

Chapter 2

2 Literature Review

2.1 Introduction

The motivation of this work is to create processing techniques to allow for the production of more complicated structures than the state of the art. This chapter introduces the materials and applications of surgical training models and their history. The area of focus for the study is PVA hydrogels, and as such, the literature pertaining to their use in medical applications is presented. Both self-healing and joining characteristics of hydrogels are reviewed. Finally molding techniques will be presented that lend to the production of complicated structures.

2.2 A Brief History of Surgical Training

Surgical training takes various forms with varying degrees of sophistication and fidelity. The development of training practices has taken place over nearly a millennium. Truly academic surgical training can be dated back to the thirteenth century, where at the University of Bologna in Italy, the dissection of cadavers was a mandatory part of the medical curriculum. The lack of appropriate preservation techniques limited the availability of cadavers so pigs and other animals were sometimes substituted [4]. University trained physicians were few in numbers, so the majority of the population relied

on so called “barber-surgeons” who had a less formal apprenticeship form of training. Barber surgeons were more akin to craftsman [5]. Without standards of training, access to medical care, specifically surgery, was inconsistent.

It would not be until the end of the nineteenth century that the apprenticeship model would merge with academic learning in North America. It was Dr. William Steward Halsted, in 1889, at The John Hopkins Hospital in Baltimore that can be credited for this merger. As chief of surgery he created a program where medical school graduates would participate in a several year training program with increasing responsibility, with a final year of near complete independence [6]. This form of training is the backbone of modern surgical residency, and allowed for the development of surgeons with both a strong scientific base and technical skills.

2.3 Modern Surgical Training Simulation

The centuries long tradition of patient based case training raises certain issues. It is reported that patient safety is negatively impacted by training in the operating room [8, 9, 7]. From the patients’ perspective it is ideal if only the most experienced surgeons performed surgeries; however, education and experience are different. For this reason surgeons must gain hands on experience to become truly capable, and this does not necessarily have to be gained entirely in the operating room. Modern surgical training involves a mixture of simulated methods, a selection of which are described below.

Live animal models are common high fidelity human analogues. Common lab animals for human study are typically mammals due to their similar organs and overall body structure.

Pigs in particular share all of the same thoracic and abdominal organs with only very minor differences from human analogues [10]. Under anesthesia, live animals provide the closest available simulation of surgery on a human patient. This type of training can be expensive due to the required operating, anesthetization, handling and post-operative equipment [11]. Legal and ethical concerns for the treatment of animals can make the justification for their use difficult over alternatives [12].

Virtual reality simulators are the most recent advance in surgical training. They provide fully safe acquisition of skills, as well as easily quantifiable assessment of learning in trainees [13]. The metrics for assessment in a simulator, such as speed and position, do not necessarily translate into the more subtle measures and emotional inputs of real world experiences, which may be more subjective [14]. For this reason, virtual reality simulators are still a very active area of development.

Laparoscopic surgery is a modern form of surgery that has benefited from extensive use of simulators. Laparoscopy or minimally invasive surgery (MIS) involves small incisions and the use of remote cameras and tools which reduce the pain and recovery associated with open procedures [15]. Simple box trainers can be used which simulate the human abdomen and contain ports for laparoscopic tools and contain anatomical features and other training tools for acquisition and practice of laparoscopic skills [16, 17].

Full surgical training models are used in all areas of surgery and replicate the human body with varying realism. Surgical training models typically mimic the anatomy and the properties of human tissues. Many models are commercially available for a wide range of procedures [18, 19, 20]. Most of these models are composed of various elastomers and

foams, often silicone, latex and polyurethane based materials [21]. These materials can typically mimic the color and complex shapes needed for models; however, they often lack representative mechanical properties of human tissues.

2.4 Hydrogels

Hydrogels are a group of materials that exhibit properties making them suitable for surgical training models and for biological applications. They are characterized by sufficient crosslinking to form gels and hydrophilic groups to allow for high water content [22]. In human, water content can range from 63 w% in tendons to 86 w% in the brain [23]. The viscoelastic behavior of hydrogels, along with high water content, makes them ideal candidates for surgical model applications.

Gelatin is a familiar hydrogel and is commonly used in medical models. Gelatin is the standard material used in ballistics model as a representation of human tissue [24]. Gelatin is essentially hydrolyzed collagen that can be dissolved in water at elevated temperatures. When cooled, the polypeptide strands aggregate into a collagen like structure forming a thermoreversible hydrogel [25]. Gelatin is accessible, cheap and easy to process with minimal equipment. It does suffer from certain drawbacks such as high variability in molecular weight from natural sources and thermoreversibility of physical gelation.

Many other hydrogel systems with interesting properties for application in surgical training models exist. Some important polymer hydrogels are alginate and polyacrylamide. Many interesting properties are obtained from blends of these polymers in the form of double network gels [26, 27].

2.5 Poly(vinyl alcohol) hydrogels

PVA is a synthetic water soluble polymer with a wide range of uses. PVA is produced by polymerization of vinyl acetate into poly(vinyl acetate), followed by partial hydrolysis to form PVA. PVA is used in a range of applications, one of its main uses is for sizing of paper and textiles [28]. The chemical structure of PVA is shown in Figure 1.

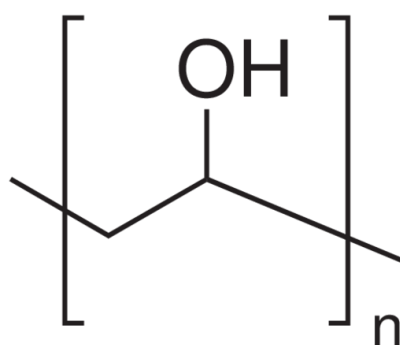


Figure 1 - Chemical structure of poly(vinyl alcohol)

The solubility and solution characteristics of PVA is dictated by both the degree of hydrolysis and the molecular weight of the polymer. Optimal solubility in water at room temperature is achieved in the range of 87-89 % hydrolysis. At higher degrees of hydrolysis, intra and inter-molecular hydrogen bonding requires higher dissolution temperatures to provide the necessary energy to form a solution. PVA solutions are more stable in partially hydrolyzed grades, where highly hydrolyzed grades readily form gels due to hydrogen bonding at room temperature. Solution viscosity increases with increasing molecular weight [29, 30].

PVA in solution with water can be crosslinked both chemically and physically. Chemical crosslinking requires the use of crosslinking agents, in general any compound that is multifunctional and can react with hydroxyl groups on the PVA chain can be used as a crosslinking agent. Some useful crosslinking agents include maleic acid, dialdehydes and boric acid [31, 32, 33]. Useful properties are obtained using crosslinking agents; however, residual crosslinking agent and generally poor mechanical properties of chemically crosslinked PVA hydrogel is not favorable for surgical models.

Physical crosslinking of PVA solution produces gels with useful properties for surgical training models and for biomedical applications in general. A novel method for physical gelation of PVA solutions was introduced by Tanabe and Nambu [34] as a patent in 1985 and work on the method can be dated as early as 1975 by Peppas [35]. The method involves freezing a solution of PVA, usually with greater than 98 % degree of hydrolysis and a molecular weight greater than 80,000 [34]. This process produces strong gels that can be easily handled and are stable up to approximately 60 °C.

The physical gelation process of PVA solutions has been studied in detail, but it is not entirely understood. It is well known that PVA solutions exhibit spontaneous gelation at room temperature, which can be attributed to crystallite formation [29]. In fact, it has been shown that prolonged heating during dissolution creates a more stable solution than one that was heated for a shorter period of time which retains more of its crystallinity [36]. It is generally accepted that during freezing a liquid-liquid phase separation occurs creating a polymer rich and polymer poor phase. The polymer rich phase itself consists of an amorphous and crystalline phase, which reinforces the three dimensional network [32, 37, 38]. The literature does not have consensus on whether liquid-liquid phase separation is

the primary driver of gelation. It is clear that the melting point of physical gels, ~ 60 °C, when compared to the much higher melting point of ~ 230 °C for unplasticized PVA, is closely tied to the endothermic peak associated with the melting of crystalline regions [39, 40]. This strongly indicates that crystalline regions act as the junction points, which reinforce the gel network.

Physically crosslinked PVA gels can be tailored based on the freeze-thaw method employed. In the freeze-thaw process polymer concentration, freeze rate, hold time, hold temperature, thaw rate and number of freeze-thaw cycles can all be varied to tailor the properties of the resulting gel. Domotenko demonstrated that slower rates of thawing and higher polymer concentrations resulted in higher elastic modulus [41]. Later Lozinsky showed that the cooling rate was less significant than the thawing rate in terms of the resulting elastic modulus of the PVA hydrogel [42]. It has been shown by many independent groups that gelation mainly occurs during thawing. It has been attributed to a region several degrees below the freezing point where sufficient chain mobility in the polymer rich region gives rise to conditions that favor gelation [43, 44, 32].

The structure of PVA hydrogels gives rise to unique mechanical properties that closely resemble biological tissues. The phase separation and growth of ice crystals that subsequently melt upon thawing leaves behind a macro-porous three dimensional hydrogel network [45, 46, 47, 48]. The open cellular network supported by solvent water mimics both the physical structure and water content of biological materials. PVA hydrogels have been shown to exhibit the nonlinear stress-strain response characteristic of biological materials, specifically porcine aortic root within the physiological strain range [49, 44]. Millon also showed that through controlled strain during freeze-thaw cycles, controlled

anisotropic properties could be achieved [50]. The ability to tailor mechanical properties to match many biological tissues make PVA hydrogels ideal candidates for surgical training models.

2.6 Adhesion

In surgical training model materials it is often desirable to form structures that are composed of materials with varying properties joined to each other. The various structures and organs of the human body are in general composed of distinct layers. For instance, the small intestine is composed of four distinct layers: mucosa, submucosa, muscularis externa and serosa [51]. There are four main types of tissues: epithelial, muscle, nervous and connective. Connective tissues are the most important to the idea of adhesion in surgical models.

As the name implies, connective tissues play a structural role in binding together the various other tissues of the body. Connective tissue consists of ground substance, fibers and cells. The ground substance, an amorphous gel complex, and fibers, mainly collagen and elastin, form the extracellular matrix of connective tissue cells. Varying proportions of the constituents exist for different areas of the body. For instance, loose connective tissue has thinly dispersed fibers and acts to connect structures while allowing significant relative movement. Dense irregular connective tissues are almost acellular and are densely packed with fibers in areas of high loading [51, 52].

Adhesion in hydrogels can be achieved by various mechanisms. When lightly crosslinked polymer surfaces come into contact, amorphous chains are mobile and able to

interpenetrate and entangle [53]. This is especially true for highly plasticized polymers such as hydrogels. Self-healing hydrogels make use of this effect when chains are sufficiently mobile across the interface to entangle and form hydrogen bonds between functional groups [54]. It was shown that increased crosslink density reduced interfacial strength in self-healing gels.

2.7 Rotational Molding and Casting

Rotational molding and casting are relatively specialized polymer processes when compared to high volume commercial methods such as injection molding. In its most basic form, a closed mold cavity is rotated to disperse material into an even layer on the mold cavity surface, which either solidifies thermally or sets chemically [55]. These methods are applied to produce products including sculptures, kayaks, hollow chocolate figurines and many more. This process lends itself well to the production of hollow structures and enclosed volumes that other processes cannot produce. This method has been employed for production of PVA hydrogel training models in this study.

2.8 Summary

PVA has been studied in great detail for its mechanical properties, applications as implantable materials and for controlled drug release. It is known that PVA is a good analogue for human tissues in terms of certain mechanical properties. In order to create useful and realistic training models methods of joining and molding complex structures have been developed and evaluated.

Chapter 3

3 Experimental Methods – Joining

3.1 Introduction

The objective of this work was to examine methods for joining PVA hydrogel materials to one another. Several techniques were employed in understanding the joining process. Firstly, the modulus of the underlying PVA hydrogels was characterized in uniaxial tension. An overmolding procedure was developed to produce consistent bonds between the base layer and the overmolded layer. A modified peel test was developed to determine the peel strength between the hydrogel layers. Porosity and crystallinity of the underlying gels was measured using differential scanning calorimetry to identify gel characteristic for freeze-thaw cycles that showed strong bonding between layers.

3.2 Material Preparation

3.2.1 Poly(vinyl alcohol) solution preparation

PVA (Sigma-Aldrich Canada Co.) was obtained with a molecular weight 146,000-186,000 g/mol, 99 %+ hydrolyzed and was used in the preparation of all solutions. 10 wt% solutions were prepared by dissolving with deionized water in a jacketed flask with condensing reflux at 90 °C for 3 hours until a homogenous transparent solution was obtained, using the procedure described previously in literature [44, 56]. 10 wt% solutions were used

exclusively throughout the study as it was considered the most relevant concentration to consider for applications in surgical training models.

3.3 Uniaxial Tensile Testing

3.3.1 Sample Preparation

The mold used to produce 190x140x2.2 mm hydrogel sheets is shown in Figure 2. The mold consists of 2 polished aluminum plates and a nylon spacer-gasket which forms the sheet cavity.

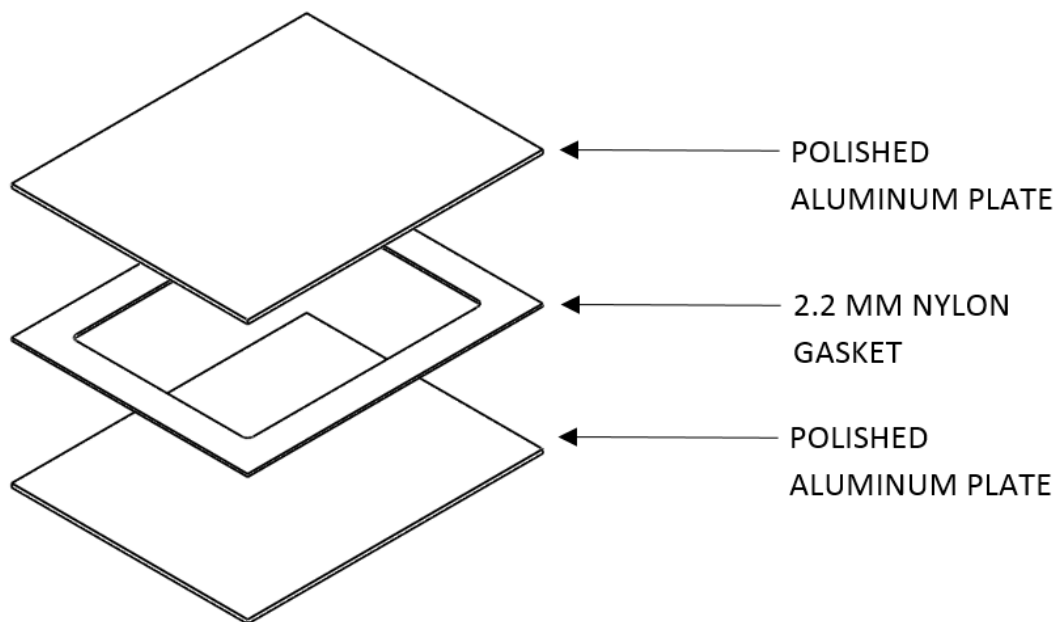


Figure 2 – Diagram of PVA injection sheet mold. Not shown is the steel binding clamps used for mold closure.

The mold components were stacked and clamped together using two 2 inch steel binding clamps per edge to provide the necessary force to resist the pressure of injection. In order

to fill the mold, a 100 ml dosing syringe was filled with PVA solution a degassed by inverting the syringe and expelling visible entrapped air bubbles, as voids caused by air bubbles will negatively impact the strength of the gel and should always be avoided. PVA was injected using the syringe until the mold completely filled.

Molds were transferred into an environmental chamber for freeze-thaw. The chamber has fully programmable temperature profiles between $-73\text{ }^{\circ}\text{C}$ and $+175\text{ }^{\circ}\text{C}$ with a control tolerance of $\pm 0.2\text{ }^{\circ}\text{C}$ and a uniformity of $\pm 0.5\text{ }^{\circ}\text{C}$ throughout the chamber. The medium of cooling in the chamber is air, so the mold material was chosen as aluminum because of its high thermal conductivity.

As stated previously, slow rates of thawing were observed to produce stiffer gels than high rates of thawing, so a rate of $0.1\text{ }^{\circ}\text{C}/\text{min}$ was used for both thawing and cooling [43]. The chamber was programmed to run 3 consecutive cycles over the course of 45 hours. After the completed cycle time a mold would be removed for tensile testing and the others would continue to cycle further. The temperature profile is given in Table 1.

Step	Duration (min)	Start Temperature	End Temperature
Cooling	400	$+20\text{ }^{\circ}\text{C}$	$-20\text{ }^{\circ}\text{C}$
Dwell Frozen	60	$-20\text{ }^{\circ}\text{C}$	$-20\text{ }^{\circ}\text{C}$
Thawing	400	$-20\text{ }^{\circ}\text{C}$	$+20\text{ }^{\circ}\text{C}$
Dwell Thawed	40	$+20\text{ }^{\circ}\text{C}$	$+20\text{ }^{\circ}\text{C}$

Table 1 – Temperature Profile for a Single Freeze-Thaw Cycle

10x50mm tensile samples were cut using an Olfa rotary cutter and a straight edge [57]. The rotary cutter was chosen because of its smooth cutting action which created flat edges with minimal defects. The more conventional punch was not used because it tends to compress the soft material leaving non-uniform edges with defect. Also, to prevent the high water content material from slipping during cutting, a paper towel was placed under the material during cutting to constrain it. The differences in cutting methods are depicted in Figure 3 and Figure 4.

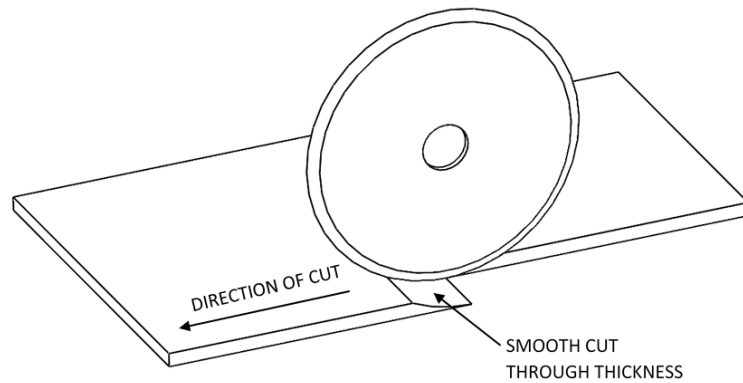


Figure 3 – Rotary cutting of tensile samples

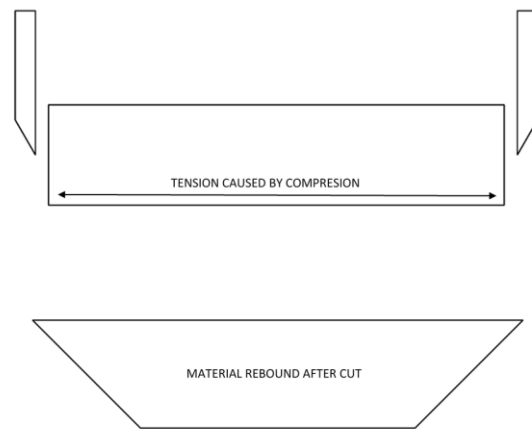


Figure 4 – Trapezoidal rebound of punch cutting samples

3.3.2 Equipment

Tensile tests were carried out on an electromechanical test stand (Mark-10 ESM301L). A customized soft tissue grip was developed for the purposes of this project. The grip body material is stainless steel with 100 grit aluminum oxide adhesive backed sand paper on the grip faces. A fixture was designed to align the grips while loading the samples to ensure accurate and repeatable alignment and spacing. The grips and alignment fixture is shown in Figure 5.

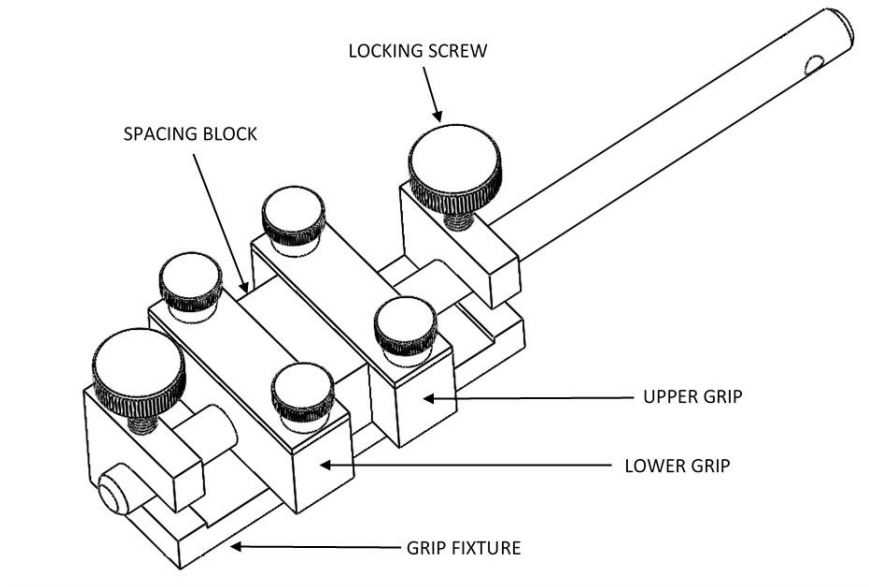


Figure 5 – Grip alignment fixture

The tensile equipment setup is shown in Figure 6. The force gauge (Mark-10 Series M5-10) collects data at a rate of 7,000 hz and transmits force data via data cable to the test stand control unit. The test reads position data from an internal linear scale, at a 50 hz data rate. The test stand then outputs force and position data simultaneously over RS-232 in ASCII format limited to 50 hz by the linear scale. Full control of the machine over RS-232 in ASCII format is possible; however, no commercial software was available for this function.

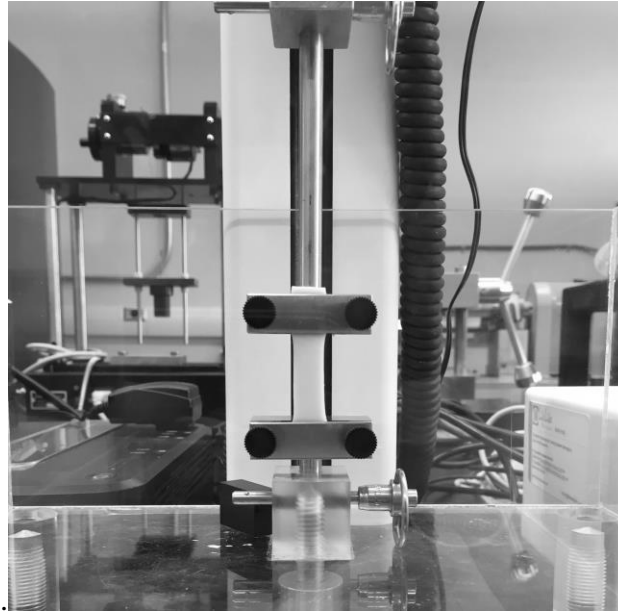


Figure 6 – Tensile soft tissue grips with 10x50x2.2mm sample

A custom program was written for both machine control and data acquisition using Microsoft Visual Studio 2010 in the Visual Basic programming language. The program was written in accordance with the ASCII command table published by Mark-10 and can be found in Appendix C: ASCII command table for ESM301L test stand. The programs user interface is shown in Figure 7.

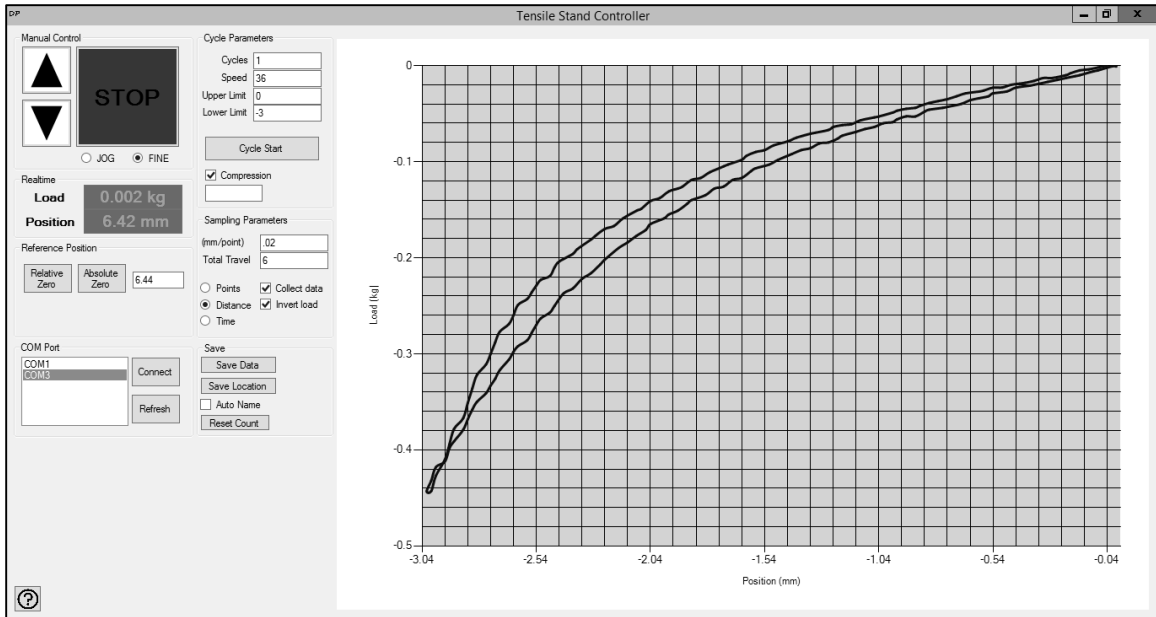


Figure 7 – User interface for tensile test stand

The program allows for setting test cycle parameters (velocity, distance, acquisition rate, units and cycles). The program exports the raw data into Microsoft Excel file format. The program also allows for manual control over the machine motions for setting of initial positions and reading real-time values.

3.3.3 Uniaxial Tensile Test

Testing was carried out in ambient conditions. Sample dimension of thickness and width were measured using digital calipers and were reported to the nearest tenth of a millimeter. Samples were loaded into the grip fixture to a gauge length of 25 mm. The force applied by gripping the samples tends to squeeze material into the gauge length. To account for this, the crosshead was manually driven until zero force reading was obtained at which point the true gauge length was recorded.

It is known that residual stress may be present in PVA hydrogels, which may give an artificially high modulus on the first loading. For that reason, the samples were preconditioned to relieve residual stress in the material and provide a uniform history of stress on the materials [50]. Samples were preconditioned to a 1.65 extension ratio at 8mm/s for 10 load-unload cycles. The crosshead was then manually driven to zero the load and take up any slack in the material from preconditioning. Data was then recorded during an additional load-unload cycle at the same strain and strain rate.

Samples were weighed in the hydrated state and dried at 110 °C on aluminum foil for 2 hours to determine the polymer fraction of the samples. The gels expel free water with increasing number of freeze thaw cycles. This increases the polymer fraction of the samples accordingly so this was taken into account to normalize the properties to the volume fraction of polymer in the samples.

3.4 Peel Strength

3.4.1 ASTM D903-98 Peel Strength Standard

In order to determine the peel strength of bonded PVA, the methods described in ASTM D903-98 were followed [58]. The standard applies to adhesive bonds where at least one of the materials is flexible and thin enough to permit the bend of 180° required for the test.

Initially a t-peel test was investigated for determination of peel strength. The forces required to peel the samples caused significant stretch in the free ends of the peeling sample. The stretch in the samples stored elastic energy which was released in a cyclical way. This cyclical release of stored energy made determination of an average peeling load

infeasible. In order to maintain a constant separation rate of the sample the materials should be inextensible and flexible relative to the peeling load.

The findings from initial testing suggested that an 180° peel test was more appropriate for a PVA hydrogel system. This is likely true for any hydrogel system where the peeling load is great enough to cause significant stretch in the material. The strain energy built in the sample is non-recoverable and is difficult to account for in analysis without prior knowledge of material properties.

3.4.2 Sample Preparation

In the 180° peel test one side of the bond has to be rigidly fixed to maintain alignment and the other should be inextensible and flexible relative to the peeling load [58]. In order to accommodate these requirements a method of preparation for hydrogels was developed. The form of the 180° peel specimen is shown in Figure 8.

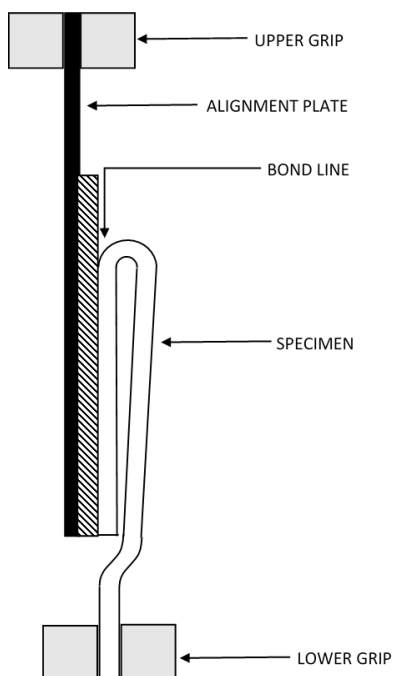


Figure 8 – ASTM D903 peel strength specimen

The flexible-inextensible side of the specimens is formed first. Flax linen was chosen as a suitable embedded material for the peel specimens to render them inextensible. Flax linen is relatively stiff compared to the hydrogels and its absorbent nature allows it to embed and bond strongly within the PVA hydrogel during crosslinking. The flax linen has 15 threads/cm in a plain weave, 0.25 mm in thickness (Fabricland Distributors Inc.). A section of linen larger than the mold was pulled taut around an aluminum mold plate and clamped in place with a nylon gasket and upper mold plate. The PVA solution was injected into the mold and cycled.

After cycling the upper mold half was removed to expose the gel surface opposite the embedded linen. The surface of the gel was tapped dry with lint free wipes to remove

pooled water that could cause variations in the bond. A second 2.2 mm nylon gasket was placed atop the first and the upper mold half was repositioned and clamped in place. A second layer of solution was injected over the first layer and cycled to create the 2 layer peel specimen.

After cycling the overmolded layer, the gel block was removed from the mold. The resulting block was dividing using a rotary cutter into 25 mm wide strips each containing a continuous strip of linen which extended beyond the gel in the length direction, as shown in Figure 9.

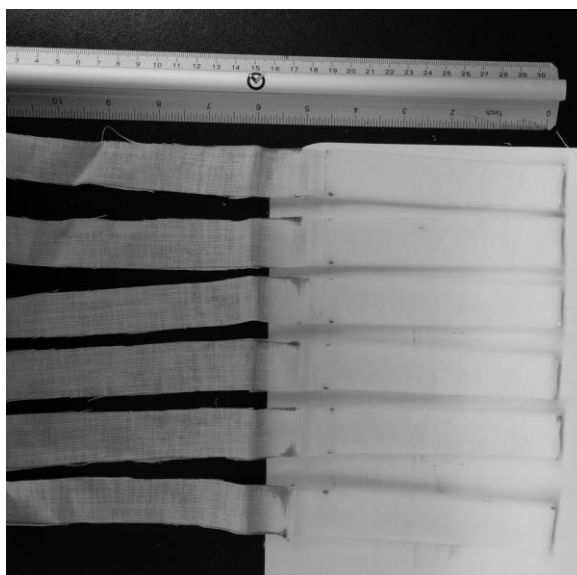


Figure 9 – Linen embedded in peel specimens before bonding to alignment plate

In order to fix the rigid side of the specimen to the alignment plate, a suitable adhesive was chosen that would bond the high water content PVA gel to polypropylene. An ethyl cyanoacrylate based adhesive (Henkel, Loctite 495) was used to bond the gel to a 3 mm

polypropylene alignment plates. Ethyl cyanoacrylate adhesives polymerize in the presence of water within seconds forming a strong bond with PVA hydrogels [59]. The polypropylene alignment plate was first prepared for the adhesive by sanding with 100 grit sandpaper. A thin layer of adhesive was spread onto the surface of the alignment plate using a tongue depressor. The peeling specimen was then placed onto the adhesive and pressed evenly in place for 30 seconds to form a strong uniform bond. Samples were then placed into a sealable specimen bag until testing to prevent drying. All samples were tested on the same day as preparation.

From tensile tests it was shown that the maximum stiffness was achieved at freeze-thaw cycle $n=7$. The variable of interest in this study was the number of freeze-thaw cycles of the base layer prior to overmolding the top layer. To isolate the variable of interest the number of freeze-thaw cycles of the base layer was varied from 1-7 and the overmolded layer along with the base layer were cycled a further 7 times. The further processing created a two layer structure with similar maximum stiffness in both layers, with the only difference being the number of freeze-thaw cycles of the base layer prior to overmolding. A summary of the samples prepared is shown in Table 2.

Sample Set	Overmolded @ cycle #	Total cycles of base layer	Total cycles of overmolded layer
1	1	8	7
2	2	9	7
3	3	10	7
4	4	11	7
5	5	12	7
6	6	13	7
7	7	14	7

Table 2 – Summary of peel samples tested

3.4.3 Testing

The weight of the specimen including the alignment plate was significant relative to the peeling loads, therefore the force gauge of the testing stand was tared with the specimen in the top grip.

The alignment plate was fixed in the top grip of the machine ensuring proper alignment with the axis of the force gauge. The free end was peeled back approximately 25 mm to initiate the peel and to allow it to bend 180° to the lower grip. The free end was gripped in the lower grip ensuring proper alignment with the force gauge axis.

The test was conducted at a grip separation rate of 305 mm/min. This separated the bond line at half of the grip separation rate, 152 mm/min, which remained constant for all tests. The load and position were recorded at 50 hz and captured for the entire travel of each test.

After testing the specimens were examined for failure type and reported. The bonds being examined could exhibit three types of failure: adhesive, cohesive and mixed mode. Cohesive failure was indicated by failure in the bulk material. Adhesive failure was indicated by smooth damage-free newly formed surfaces. Mixed mode failure is identified by residual material on the newly formed surface caused by distinct regions of both adhesive and cohesive failure. Cohesive failure is considered to be a strong bond as this indicates the bond has similar strength to the bulk material [60].

3.5 DSC

3.5.1 Introduction

When similar partially crosslinked polymers are brought into contact a bond may be formed by interdiffusion across the interface. In general, a stronger bond is achieved from a lesser degree of crosslinking and greater contact time [53]. A decrease in bond strength with increasing freeze-thaw cycles (greater degree of crosslinking) was not observed in this work as would be expected, so an investigation of crystallinity and porosity was completed. Measurements we made using differential scanning calorimetry (DSC). Crystallinity measurements were made following the methods described by Riccardi et al [61]. Porosity measurements were made adapting the methods of Plieva et al [62].

3.5.2 Equipment

Measurements were made using a TA instruments Q2000 differential scanning calorimeter. DSC maintains the temperature difference between a reference and the sample close to zero and measures the difference in energy input needed to maintain that balance in temperature. The reference being an empty specimen pan means that the difference in energy is attributed to heat absorbed or evolved by chemical or physical changes caused by a linear temperature ramp [63].

3.5.3 Sample Preparation

PVA hydrogel sheets, 190x140x1 mm were prepared using polished aluminum plates molds and nylon gaskets. PVA solution was injected into the void between the gasket and

plates, clamped and transferred into the environmental chamber for processing. After freeze-thaw cycling the thin PVA sheets were placed into sealable specimen bags prior to testing. All samples were tested the same day freeze-thaw cycling was completed to minimize any effect of aging.

3.5.4 Testing

The PVA gel sheets were removed from the bag and placed onto plastic cutting board. A 4mm steel punch and dead-blow hammer were used to cut DSC specimens from the sheets. Using tweezers to minimize contact, a hermetic pan and lid (TA Tzero aluminum) were weighed using an analytical balance to the nearest 0.01 mg. The sample was then loaded into the pan ensuring it had made flat contact with the pan bottom for consistent transfer of heat during the measurement. The lid was then positioned and crimped hermetically using the Tzero press and die set. The sealed pan was then weighed to determine the sample mass.

After weighing and sealing all of the DSC specimens, they were loaded into the autosampler carousel of the DSC machine. At all times samples were kept clean and free of any residue or contamination. Specimens were typically 10mg in the hydrated state.

For the crystallinity measurements, samples were equilibrated at 10 °C and held isothermal for 1min. The temperature was then ramped at 10 °C/min from 10 °C to 110 °C. The heat flow versus temperature was recorded for analysis in universal analysis software (TA instruments).

For the porosity measurements, samples were equilibrated at $-30\text{ }^{\circ}\text{C}$ for and held isothermal for 1 min. The temperature was then ramped at $5\text{ }^{\circ}\text{C}/\text{min}$ from $-30\text{ }^{\circ}\text{C}$ to $30\text{ }^{\circ}\text{C}$. The heat flow versus temperature was recorded for analysis in universal analysis software (TA instruments).

After DSC measurements samples were removed from the autosampler and re-weighed to check for possible failure of the hermetic seal. The sample pans lids were then punctured using a steel needle to allow water vapour to escape. The samples were dried in a laboratory oven for 1 hr at $120\text{ }^{\circ}\text{C}$ to determine the polymer fraction.

3.6 Dissolution of PVA hydrogel

3.6.1 Introduction

PVA is soluble in water and without reinforcing junction zones in the form of crystallites, PVA hydrogels would inevitably return to a solution state. It has been shown in chemically and physically crosslinked PVA hydrogels that small crystallites, which are more prevalent at lower degrees of crosslinking, are susceptible to dissolution and therefore effect the stability of PVA hydrogels [64, 65]. The stability of PVA hydrogels was measured by determining the loss of polymer from gels stored in deionized water as compared to the gels as made.

3.6.2 Sample Preparation

PVA hydrogels were produced in the conventional way, molding in aluminum molds to produce 2.2 mm thick sheets. The sheets were then removed from the mold and round

samples 12mm in diameter were cut from the sheets using a steel punch and dead-blow hammer. Samples were then stored in a re-sealable bag prior to testing.

3.6.3 Testing

For each freeze-thaw cycle 6 specimens were cut for testing. Three specimens were analyzed for polymer fraction as-made and after storage in deionized water for 180 minutes. The samples were all weighed in their hydrated state to the nearest milligram. The as-made samples were then immediately dried at 120 °C for 2 hours to remove the water from the samples. The other 3 samples were immediately stored in a segmented tray filled with deionized water at ambient conditions.

After 180 minutes the specimens were removed and immediately dried at 120 °C for 2 hours. When drying was completed the dry specimens were reweighed to determine the polymer fraction of the samples.

Chapter 4

4 Experimental Methods – Rotational Molding

4.1 Introduction

Complex structures, specifically enclosed volumes, are difficult to mold by current injection molding methods. Rotational molding was investigated as a method to produce hollow thin walled structures from PVA hydrogels. Rotational molding is a process well understood in thermoplastics, thermosets and even with food products such as chocolate. The physical crosslinking method used raises challenges that are not easily solved by current methods. Namely, the polymer solution will not physically cure in short periods at ambient conditions.

4.2 Thickening Agent

The viscosity of PVA in a 10 w% solution at room temperature is similar to liquid honey, approximately 5,000 cP. At such a low viscosity it would be impossible to rotationally mold PVA solution to a consistent wall thickness.

To produce a consistent wall thickness, fumed silica was used as a thickening agent to produce a stable paste at room temperature. Fumed silica is a branched chain-like agglomerate of silica. Its branched structure gives it a low bulk density and high surface area. The surface of fumed silica contains silanol groups, a functional OH group bonded to a silicon atom. Silanol groups interact through hydrogen bonding with other silanol groups and with polar solvents, such as PVA solutions. Fumed silica can be easily dispersed in PVA solutions and the resulting solution exhibits thixotropy.

Through hydrogen bonding the fumed silica aggregates rearrange to form a three-dimensional network, which thickens and gels PVA solutions at appropriate addition levels. When stressed or heated the network fumed silica structure breaks down, reducing the viscosity of the solution. After removing stress and heat the three-dimensional network again forms stabilizing the gel. This property allows for the PVA solution to be dispersed into a rotational mold at elevated temperatures, 90 °C, and then slowly cooled to room temperature forming a consistent stable wall thickness.

4.3 Rotational Molding Machine

A rotational molding machine was designed and constructed for the purposes of this study. The rotational molding machine consisted of two square frames which rotate within one another on perpendicular axes. The framing of the machine was constructed from ABS plumbing pipe with aluminum shafts. The frames were driven by ANSI #35 chain and sprockets which could be interchanged to adjust the relative rotation rate between the inner and outer frames. The rotational molding machine is shown in Figure 10.



Figure 10 – Rotational Molding Machine

The rotation rate of the frames is critically important to produce consistent wall thickness throughout the part. Depending on the relative rates of rotation, certain surfaces of the mold will be preferentially oriented in the direction of gravity for a greater time than others. For instance, if the inner and outer frames rotate at the same rate, the initially vertically oriented surface of the mold will never cross the horizontal plane, producing a heavily skewed wall thickness. The uniformity of the motion of the molding machine can be determined by analysis of the rotational axes. The axes of the molding machine are shown in Figure 11.

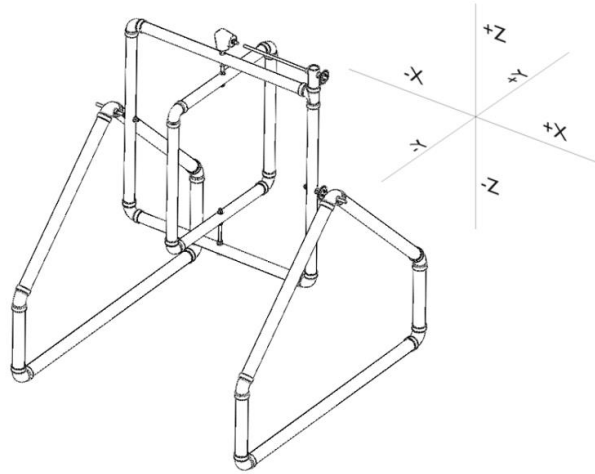


Figure 11 –Rotation axis of molding machine

The rotational matrices that describe the motion of the rotating frames are given by equation 4-1 and 4-2, where α is the rotation angle about the x-axis and γ is the rotation angle about the z-axis.

$$R_x(\alpha) = \begin{bmatrix} 1 & 0 & 0 \\ 0 & \cos\alpha & -\sin\alpha \\ 0 & \sin\alpha & \cos\alpha \end{bmatrix} \quad 4-1$$

$$R_z(\gamma) = \begin{bmatrix} \cos\gamma & -\sin\gamma & 0 \\ \sin\gamma & \cos\gamma & 0 \\ 0 & 0 & 1 \end{bmatrix} \quad 4-2$$

The ratio of α / γ is the gearing ratio of the frames of the molding machine. The gearing ratio can be modified by changing the sprocket set on the drive mechanism. The trace of an initially vertical unit normal vector on the mold surface was analyzed to determine an appropriate ratio to produce a uniform part wall thickness. The trace can be plotted from the product of the two rotational matrices by the positive z-unit normal vector over a series of angles, as shown in equation 4-3.

$$R_{x,z}(\alpha, \gamma) = \begin{bmatrix} \cos\gamma & 0 & 0 \\ \sin\gamma\cos\alpha & \cos\gamma\cos\alpha & -\sin\alpha \\ \sin\gamma\sin\alpha & \cos\gamma\sin\alpha & \cos\alpha \end{bmatrix} \begin{bmatrix} 0 \\ 0 \\ 1 \end{bmatrix} \quad 4-3$$

By plotting the trace of the initially vertical unit normal vector the importance of the gear ratio becomes obvious. The traces for three possible gear ratios are shown in Figure 12.

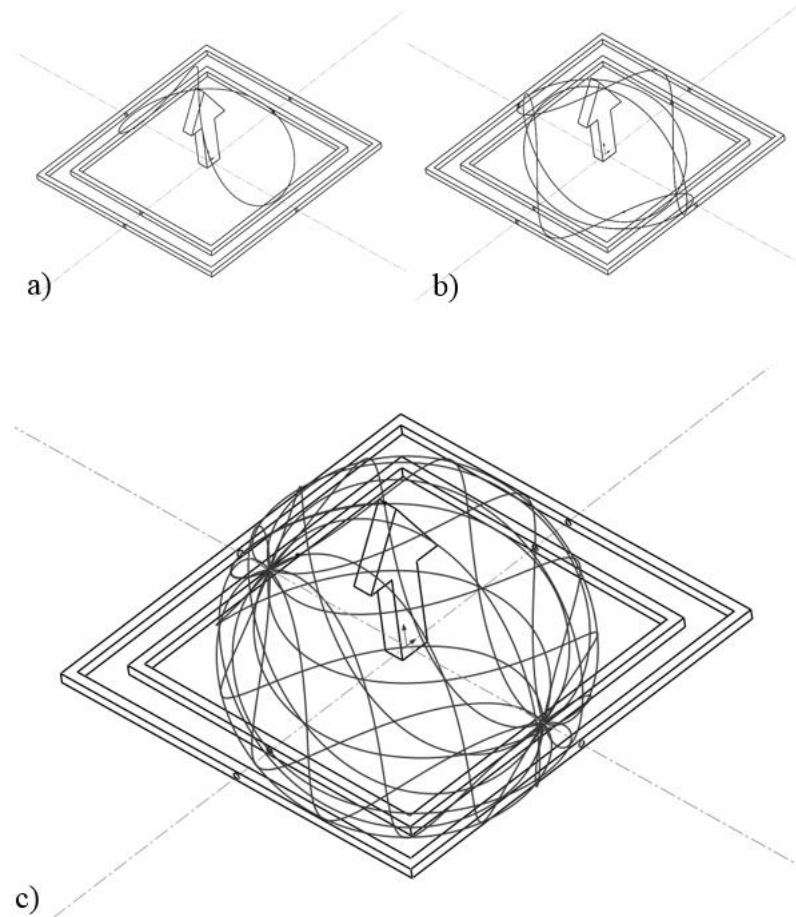


**Figure 12 – Trace of mold orientation for select gear ratios (outer:inner)
a) 1:1 b) 1:1.5 c) 1:22**

It is clear from the cyclical paths shown that choosing an appropriate gear ratio will yield better path uniformity. The 1:22 gear ratio was used for all testing, this was accomplished by using an 18 and a 22 tooth sprocket, i.e. the inner frame rotates 11 times for every 9 rotations of the outer frame.

4.4 Mold Making

Rotational molds are typically two part molds which form a hollow cavity. Unlike cavity-core type molds that may be used in injection molding, wall thickness is determined by the amount of material added to the mold during processing. The rotational molding of thickened PVA solution is performed at moderate temperature, usually less than 100 °C. This allows for the use of vacuum formed thermoplastic molds, which can withstand the moderate temperatures.

The techniques for PVA rotational molding were inspired by chocolate molding [66]. Molds used for chocolate are often food-grade polycarbonate (PC) or polyethylene terephthalate (PET) [67]. These molds are typically made by thermoforming sheets around a positive form of the desired shape, producing a two part negative mold cavity.

The demonstrator part in this study was a human stomach. The stomach consists of a large hollow body connected at the top and bottom to the esophagus and duodenum respectively. The diameter of the stomach body is much larger than its opening. It would be very difficult to mold the hollow cavity with a core making it an ideal structure for rotational molding. The stomach geometry was modeled using computer aided design (Dassault Systèmes, SOLIDWORKS 2014) based on general dimensions obtained from literature as shown in [68, 69].

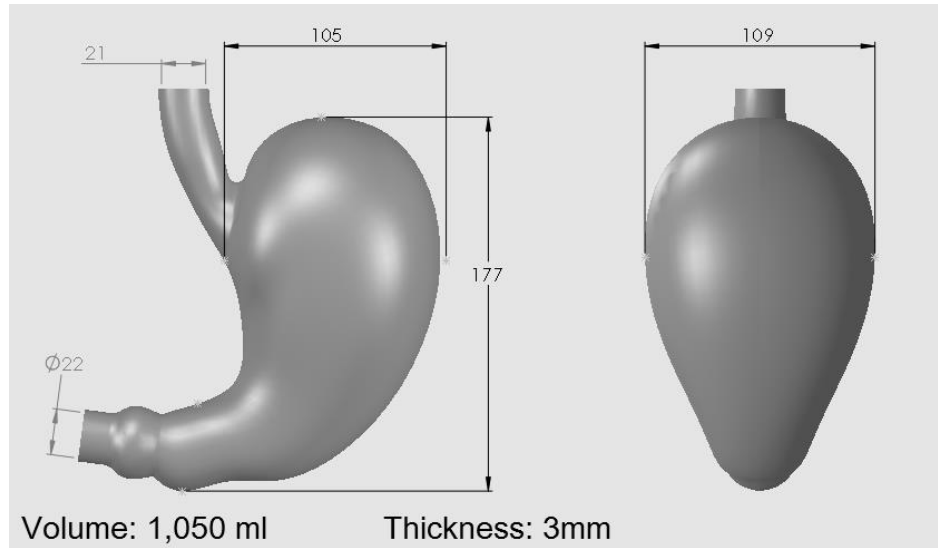


Figure 13 – CAD model of stomach demonstrator part

After creating the geometry of the stomach model in CAD, it needed to be produced in two halves that could be subsequently used to make the molds by vacuum forming. To produce the split geometry, rapid prototyping was used. The geometry was segmented into two halves in design software and alignment pins were added on the periphery. The molds were rapid prototyped in ABS plastic by fused deposition modeling (FDM) on a 3D printer (CubePro Duo, 3D Systems). The printed models, which are mirror images of one another, are shown in Figure 14.

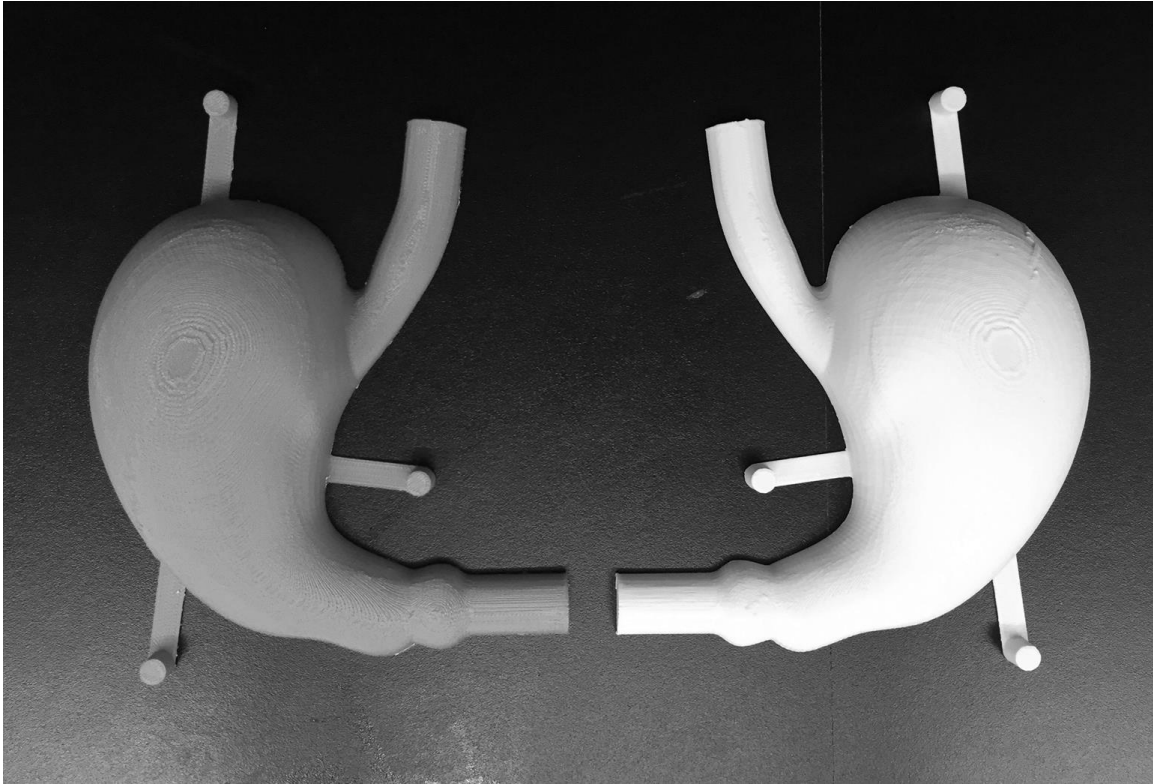


Figure 14 – FDM printed stomach positives in ABS plastic

The rapid prototype models had a slightly rough surface, due to the finitely thin printed layers, which was smoothed using 220 grit sand paper prior to vacuum forming.

In order to obtain the best feature definition from vacuum forming the thinnest reasonable plastic was used as it would deform easier under the vacuum pressure. White 0.8 mm high impact polystyrene (HIPS) was used for vacuum forming. HIPS was readily available and is one of the easiest plastics to thermoform. The vacuum former used in this study was a Centroform EZFORM (model LV 1827) as shown in Figure 15.

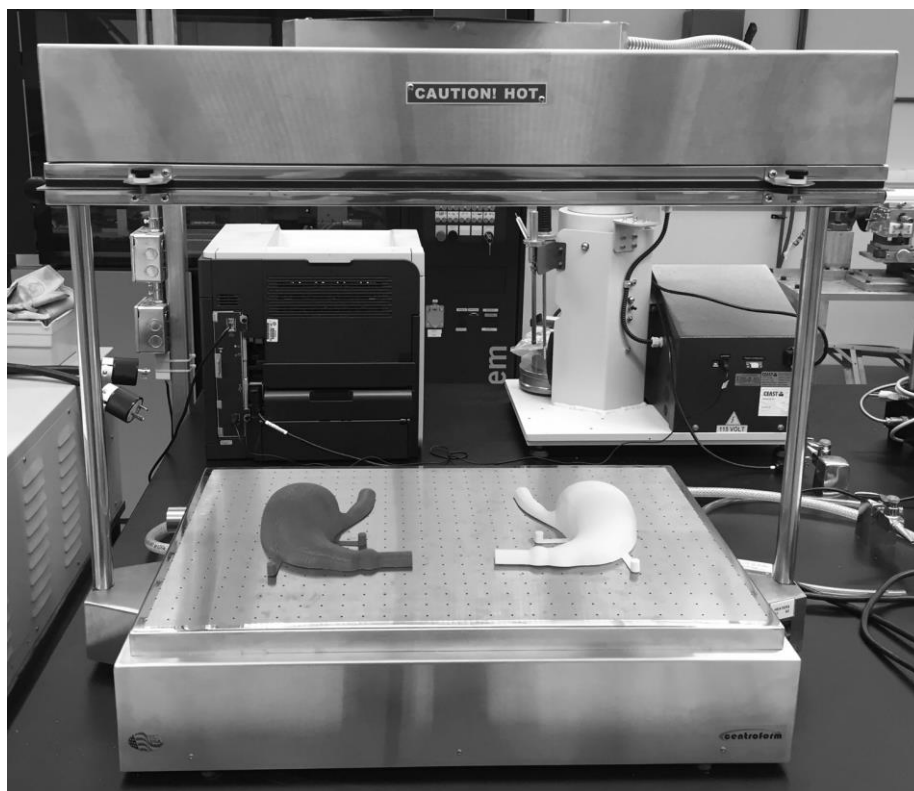


Figure 15 – Centroform EZFORM model LV 1827 with stomach positive forms

The vacuum former consists of a heater, sheet clamping frame and vacuum table. The plastic sheet was clamped in the frame and locked in position under an electrical heater above. The sheet was heated for 50 seconds until it began to sag. Vacuum was applied to the vacuum table using the laboratory vacuum supply. The sheet was then lowered over the form and the air evacuated drawing the sheet down tightly. The sheet was then allowed to cool until solid. After cooling the positive forms were easily removed, helped by a pre applied general purpose release agent (Smooth-On, universal mold release).

The vacuum formed sheet was then separated from the continuous sheet to produce the two mold halves. The cavities were trimmed from the sheet leaving a 25 mm flange for

clamping and sealing the mold. Three round aluminum alignment pins were also installed using 2-part epoxy glue. The trimmed mold halves are shown in Figure 16.

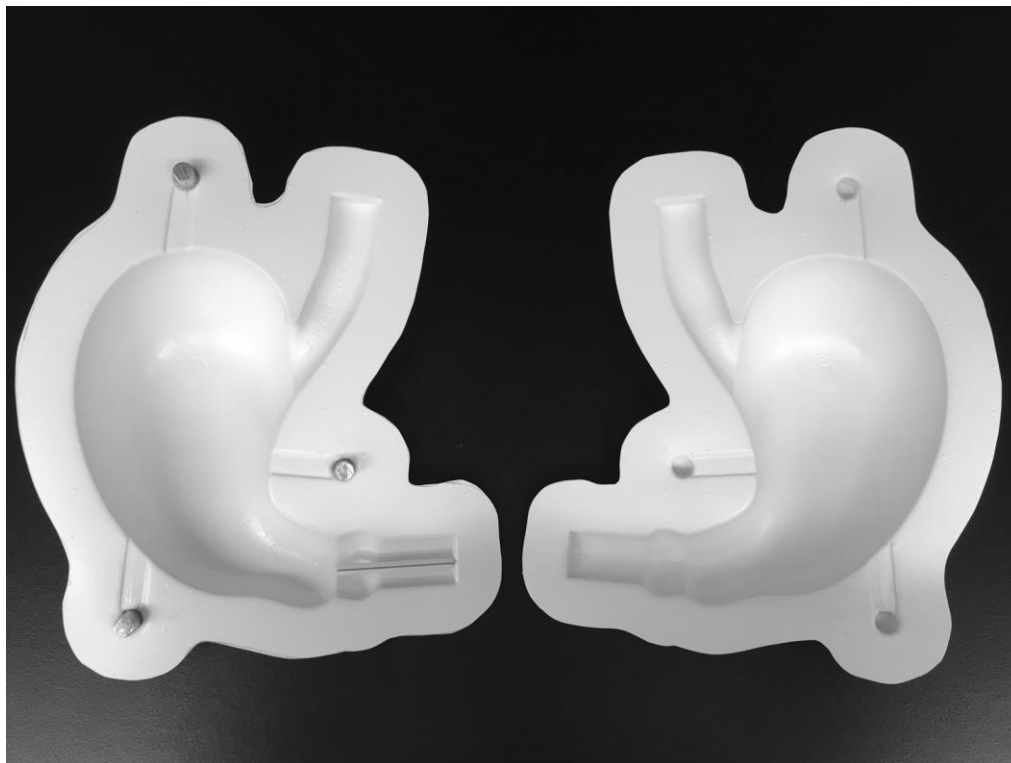


Figure 16 – Stomach mold halves, 0.8mm HIPS

4.5 Material Preparation

The fumed silica thickening agent was dispersed into the PVA solution prior to molding. Fumed silica could not be added to the 10 w% PVA solution at room temperature, as the viscosity was simply too high.

The PVA solution was first heating in a 1L water jacketed glass flask with cold water condensing reflux to 90 °C. The solution was constantly stirred with an overhead mixer

connected to a glass shaft and Teflon impellor to prevent skin formation. The fumed silica was weighed and added to the PVA solution and the stirring continued for 10min until the fumed silica was incorporated and well dispersed into the solution. Fumed silica was added in the proportions shown in Table 3.

Solution	PVA Concentration (weight %)	Fumed Silica (Part per hundred)	Freeze-Thaw Cycles
1	10	1	3
3	10	3	3
4	10	5	3
5	10	4	3
6	10	4.5	3
7	10	4.25	3

Table 3 – Fumed silica thickener additional levels

4.6 Molding

In order to produce a desired thickness, the appropriate amount of material needed to be measured out for molding. For the stomach model the outer surface of the CAD model was measured for its surface area, which is 668 cm². For an average wall thickness of 2 mm, this corresponds to a total material volume of 134 cm³.

One mold half was placed on a scale and solution containing the fumed silica thickener was added by weight corresponding to the desired volume. The second mold half was positioned and clamped in place as shown in Figure 17.

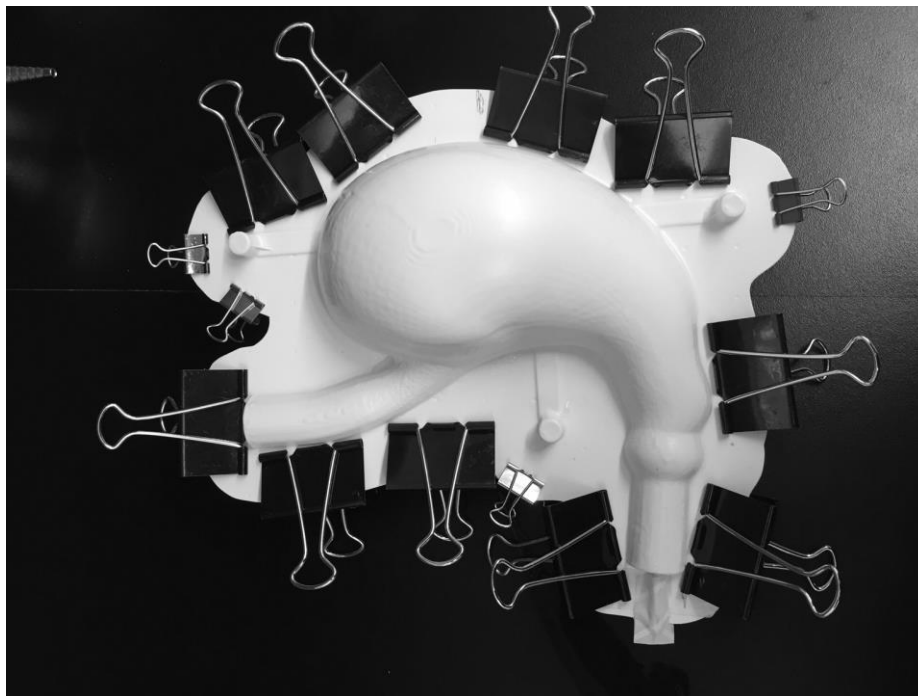


Figure 17 – Stomach mold clamped prior to rotomolding

The mold was then clamped to the inner rotational molding frame. The rotational molder was then manually turned for 20 minutes, dispersing the material on the walls of the mold until it had cooled to ambient conditions. The mold was then transferred into the environmental chamber and held at $-35\text{ }^{\circ}\text{C}$ for 30 min to quickly freeze the mold and prevent any creeping of the material. Cycling was then continued in the usual way for 3 cycles, omitting the controlled $0.1\text{ }^{\circ}\text{C}/\text{min}$ freezing at the beginning of the first cycle.

Chapter 5

5 Data Analysis

5.1 Uniaxial Tensile Testing

5.1.1 Stress Strain

From the tensile tests raw data was collected as load and position. In order to make meaningful intrinsic material comparisons, the raw data was converted into a stress strain relationship. Also, to account for variations in polymer content from loss of water during cycling, the data was further normalized to the polymer volume fraction of the samples. PVA hydrogels are in general highly extensible, with stretch ratios nearly two times their original length.

There is not a universally accepted stress-strain definition for hydrogels used in the literature. Stress definitions used for hydrogels include engineering, true, and 2nd Piola-Kirchhoff. For strain, definitions often include engineering, true, Green-St. Venant and Almansi-Hamel [70, 71, 72]. Engineering stress-strain is not a suitable for characterization of hydrogels as it does not account for deformation in the specimen, which clearly needs to be considered with extensions of up to 75 % of the original length during testing.

True stress provides instantaneous load of instantaneous area when volume is conserved, which for PVA hydrogels, having a Poissons ratio of nearly 0.5, is a valid assumption [73]. True strain provides the instantaneous change in instantaneous gauge length. All values in this study are calculated and reported under the true stress-strain definition, it is important

to consider the definition of choice when comparing this work to the literature. The definition of true stress-strain is given by equations 5-1 and 5-2.

$$\sigma_T = \frac{P}{A_0} \left(1 + \frac{\delta}{L_0}\right) \quad 5-1$$

$$\varepsilon_T = \ln\left(1 + \frac{\delta}{L_0}\right) \quad 5-2$$

Where:

σ_T = true tensile stress

P = Load

A_0 = original cross-sectional area

δ = change in length

L_0 = original length

ε_T = true strain

5.1.2 Curve Fitting

Analysis of the raw data gives stress-strain data points and many different curves can be fitted satisfactorily through these points. Equations 5-3, 5-4 and 5-5 are several empirical models that have been used extensively in the literature [56, 50, 44]. Tensile data in this study was fitted using equation 5-5, a 5-parameter exponential model. Analysis of the data initially showed equation 5-3 to consistently overestimate stress at low strains and 5-4 to underestimate at low strains. The model should pass nearly through the origin, at zero strain which was best demonstrated best by equation 5-5.

$$\sigma_T = y_0 + ae^{b\varepsilon_T} \quad 5-3$$

$$\sigma_T = y_0 + a\varepsilon_T + be^{c\varepsilon_T} \quad 5-4$$

$$\sigma_T = y_0 + ae^{b\varepsilon_T} + ce^{d\varepsilon_T} \quad 5-5$$

Where 'y₀', 'a', 'b', 'c' and 'd' are the fitting parameters.

The purpose of fitting the stress-strain data was to provide an equation from which stress values could be extracted for statistical comparison and so that slope (modulus) could be derived. The modulus is the slope of the tangent at a particular location along the stress-strain curve. The stress strain curve is non-linear in nature, and as a result so is the equation of the modulus. The modulus can be determined from the first derivative of the stress model with respect to strain as shown in equation 5-6.

$$E = \frac{d\sigma}{d\varepsilon} = abe^{b\varepsilon_T} + cde^{d\varepsilon_T} \quad 5-6$$

Data was recorded up to a true strain of 0.56, which is equal to a stretch ratio of 1.75. Values of stress and tensile elastic modulus can be interpolated between 0-0.56 strain values.

5.1.3 Polymer Fraction

It is important when making comparisons of tensile modulus in hydrogels to account for the variation in polymer fraction caused by water loss. It is assumed that the PVA network bears the load in the sample under tension. Weight loss on drying was used to determine the polymer fraction of the gels and was calculated from equation 5-7.

$$\phi_P = \frac{f_{W,P}}{f_{W,P} + \frac{\rho_P}{\rho_S}(1 - f_{W,P})} \quad 5-7$$

Where $f_{W,P}$ = weight fraction polymer (PVA)

ρ_P = density of polymer (PVA)

ρ_S = density of solvent (water)

From the strain energy, the energy stored per unit volume in the polymer phase can be calculated as shown in equation 5-8.

$$\frac{U_0}{\phi_P} = (U_0)_P = \frac{1}{\phi_P} \int_0^\varepsilon \sigma d\varepsilon = \int_0^\varepsilon \frac{\sigma}{\phi_P} d\varepsilon \quad 5-8$$

Where U_0 = strain energy per unit volume
 $(U_0)_P$ = strain energy per unit volume polymer

This means that the stress and stiffness in the polymer phase at a particular point can be found by dividing the calculated value in the bulk material by the volume fraction of the polymer. This can then be normalized to the nominal polymer volume fraction, which in the case of these experiments is 8.54 % for a 10 % target weight fraction. The normalized values for stress can be calculated as shown in equation 5-9.

$$(\sigma_T)_n = \frac{\sigma_T}{\phi_P} * 0.0854 \quad 5-9$$

Where $(\sigma_T)_n$ = stress normalized to a 10 w/% PVA

This allows for direct comparison of tensile properties of hydrogels at different cycles and accounts for the variation in water loss. Without normalization it is impossible to determine whether the difference in tensile properties between cycles is from changes in the PVA network or simply a higher fraction of polymer in the sample.

5.1.4 Analysis of Variance (ANOVA)

For statistical comparisons, one way analysis of variance (ANOVA) was used. ANOVA allows for the comparison of means between groups. Using ANOVA, with a degree of certainty, it can be determined whether the difference between group means is due to random error or due to the treatment imposed on the group. Typically, ANOVA is used on 3 or more groups, however when used on 2 groups it becomes equivalent to the Student's t-test [74].

In the analysis of tensile data, the average stress values at true strain point 0.3 and 0.5 were used for comparison. The stress values obtained at these points are assumed to be normally distributed, independent and have similar variance between groups which are necessary assumptions for ANOVA. A standard significance level of $\alpha = 0.05$ was used. The calculated F-statistic was then calculated and compared to the critical F-value. If $F > F_{\text{critical}}$ then the null hypothesis (all population means equal) was rejected.

5.2 Differential Scanning Calorimetry

5.2.1 Crystallinity

Crystalline melt out is broad for PVA hydrogels, ranging from ~40-90 °C, depending on the cycle number. At lower cycles, where the crystalline fraction is lower, there is a less obvious endothermic peak. Values of crystallinity for various cycles from different authors can be inconsistent. Many factors affect crystallinity including, but not limited to: molecular weight, free-thaw rates, DSC heating rates, specimen size and polymer fraction.

The enthalpy of fusion was found using flat baseline integration in Universal Analysis 2000 software (TA instruments), the value from integration was recorded in J/g of the hydrogel. The value was then normalized to the polymer weight fraction found from drying the sample post-test, as calculated from equation 5-7. The normalized values were then used to estimate the fraction of crystalline PVA by comparing to the value of 100 % crystalline PVA ($\Delta H_m^0=138.6$ J/g), as determined by equation 5-10 [75].

$$f_c = \frac{\Delta H_m}{\Delta H_m^0 * \phi_p} \quad 5-10$$

Where ΔH_m = the heat of fusion measured from DSC
 ΔH_m^0 = the heat of fusion of 100% crystalline PVA
 ϕ_p = the polymer fraction of the gel

5.2.2 Porosity

PVA hydrogels are porous in nature. The gels contain polymer rich and polymer poor phases. The polymer rich phase is comprised of the partially crystalline PVA network, which itself is swollen by bound water. This bound water interacts through hydrogen bonding with the hydroxyl groups of the PVA polymer chain and is not available to freeze. The polymer poor phase is defined as the pores of the gel. It is a dilute solution of free water and PVA, which is able to freeze due to the low concentration of polymer.

The relative proportions of PVA, bound water and free water can be determined using DSC. The methods of Plieva et al. were used for the analysis of porosity [62]. The heat of

melting was determined by sigmoidal horizontal baseline integration using Universal Analysis 2000 software (TA instruments). The heat of transition was recorded in J/g of the sample. After drying the samples to determine the polymer fraction, the fraction of bound water could be determined from equation 5-11 [62].

$$f_{w, \text{bound water}} = 1 - \varphi_p - \frac{\Delta H_{gel}}{\Delta H_{water}^0} \quad 5-11$$

Where ΔH_{gel} = heat of transition recorded from DSC

ΔH_{water}^0 = heat of fusion of melting ice (334.45 J/g)

φ_p = polymer fraction of the sample

$f_{w, \text{bound water}}$ = weight fraction of bound water

Knowing the mass fraction of bound water and polymer allow for the calculation of free water in the sample normalized to 10 w% PVA as shown in equation 5-12.

$$f_{w, \text{free water}} = 90\% \text{ total water} - \frac{f_{w, \text{bound water}}}{\varphi_p} * 10\% \text{PVA} \quad 5-12$$

$f_{Free \text{ Water}}$ = Free water weight fraction normalized to 10% PVA

φ_p = polymer fraction of the sample

$f_{w, \text{bound water}}$ = weight fraction of bound water

The porosity of the sample is closely tied to the hydration of the gel. It is misleading to report raw porosity values, instead it is more useful to report the bound water normalized to the polymer fraction, which allows for comparison between freeze-thaw cycles. A low value of bound water indicates a well incorporated, dense PVA gel network in the polymer rich phase.

5.3 Peel Strength

The determination of peel strength was made using the methods outlined in ASTM D903 [58]. On the load versus extension curve of the test initially the force rises to a maximum point at which steady state peeling then progresses. The arithmetic mean of load is calculated from the raw data to give an average peeling load. This load is then divided by the width of the peeling specimen to give the peeling strength in kg/mm as described in equation 5-13.

$$Peel\ Strength = \frac{1}{n} \sum_{i=1}^n P_i / w \quad 5-13$$

Where P_i = load at a particular point during steady peeling
 n = number of load data point recorded during steady peeling
 w = width of the peeling sample

Samples which failed cohesively or in mixed mode failure were reported as such, and no peeling load could be reported. In such cases this indicated the bond was of similar strength to the bulk material on either side of the interface.

5.4 Stability of PVA hydrogel

The stability of PVA hydrogel was measured as the amount of polymer lost by gels stored in a medium of deionized water under ambient conditions. This is simply the weight of a specimen after removal of water by drying compared to its weight in the as-made state.

The polymer volume fraction is then determined as described previously in equation 5-7.

Chapter 6

6 Results and Discussion

6.1 Introduction

In this chapter the experimental results of this study are presented. Each set of results are followed by a discussion of the interpretation and implications of the results.

In this section the results of tensile, peeling, crystallinity, porosity and rotational molding will be presented. Additional results (not presented in this section) can be found in the appendices at the end of the report.

6.2 Uniaxial Tensile

6.2.1 Stress-Strain

The stress-strain curves for 10 wt% PVA hydrogel at freeze-thaw cycles 3, 6, 7, 9 and 12 are presented in Figure 18. There is a clear trend of increasing material stiffness with increasing freeze-thaw cycles. The non-linear stress strain response is also visible, which is similar to natural tissues, making them ideal for tissue models.

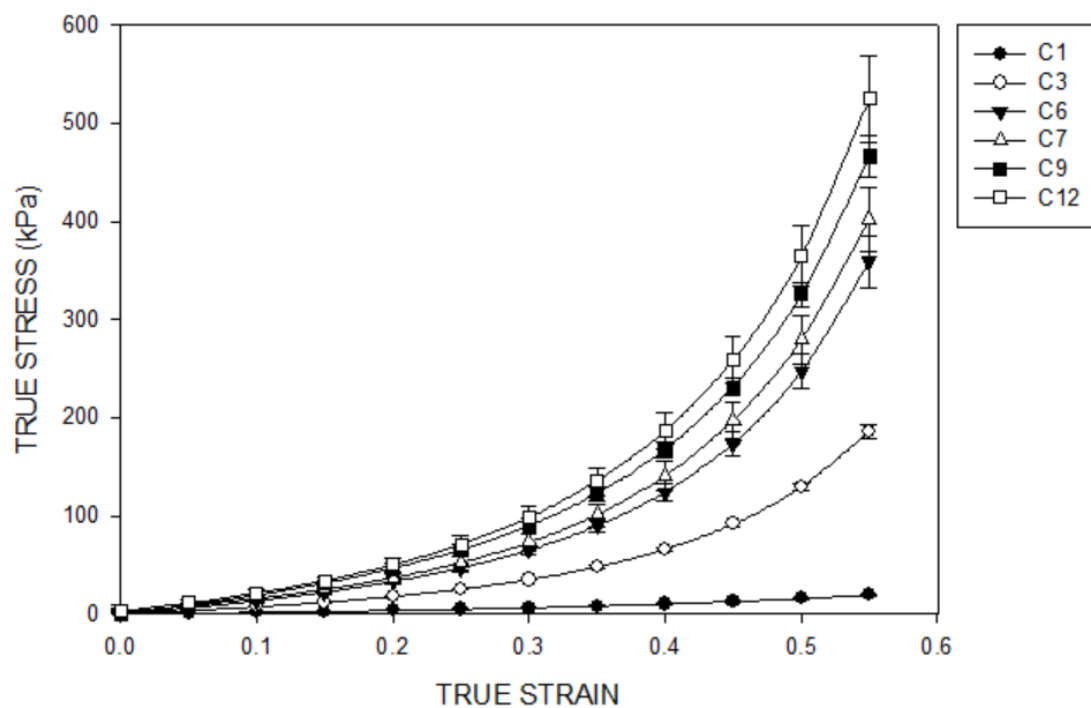


Figure 18 – Uncorrected tensile response for 10 w/% PVA

The purpose of the tensile evaluation was to determine the freeze-thaw cycle at which no more increase in stiffness was observed. At this point we can assume that further PVA network densification is not occurring and this determines the upper limit of freeze-thaw cycles that was used for the remainder of the study. As discussed previously, the stress-strain response was corrected for water loss and then normalized to a 10 w% nominal polymer fraction. This allowed for direct comparison between cycles regardless of water loss which was apparent from shrinkage in the mold as well as free water surrounding the gel sheet. The corrected stress-strain response is shown in Figure 19.

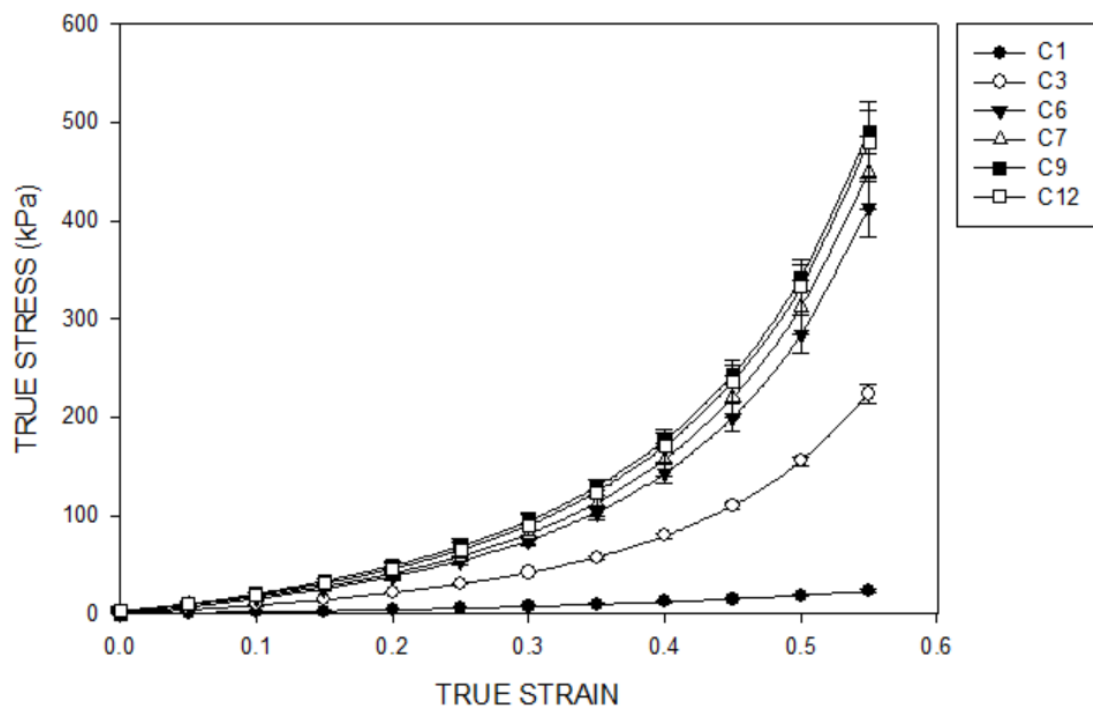


Figure 19 - Tensile response for 10 w/% PVA corrected for water loss

From the corrected tensile response, it is clear that the curves begin to group tightly above freeze-thaw cycle $n = 6$. Analysis of variance (ANOVA) did not suggest that there was a significant difference at strain values of 0.3 and 0.5 for a significance level of $\alpha = 0.05$. It is assumed that cycle 7 then represents the upper limit for stiffening of the PVA network. As water loss increases it is likely that the non-linear stress response will dissipate as the material loses its porous hydrated structure. In practice 6 cycles may be sufficient, but for the purposes of this study up to and including cycle 7 is seen as significant to changes in PVA network properties.

6.2.2 Water Loss

As described in the previous section, water loss in the samples plays a vital role in the properties of the molded PVA hydrogel. In the molding setup used for the tensile samples the gel is unconstrained and able to shrink freely. Water that escapes the sample typically remains in the mold and is cleared after demolding. Table 4 shows the water loss at various cycles for injection molded 2.2 mm plates.

Cycle	0 (Sol.)	1	3	6	7	9	12
PVA Weight %	11.0 ± 0.7	11.2 ± 0.7	11.1 ± 0.6	11.6 ± 0.8	11.9 ± 0.8	12.6 ± 0.4	14.5 ± 0.3
PVA Volume %	9.40 ± 0.6	9.57 ± 0.6	9.48 ± 0.5	9.91 ± 0.3	10.2 ± 0.6	10.8 ± 0.4	12.5 ± 0.3

Table 4 – PVA content hydrogels at various cycles for tensile correction

The targeted nominal value of the PVA solution was 10 w%. A nearly 1 % difference in the actual solution was observed after cooling to room temperature overnight before molding. This is likely due to condensing water that has to be removed from the jars after cooling and water that is lost as humidity through the condensing reflux. Adjustments can be made post cooling; however, as long as the methods of preparation are kept consistent and the true values recorded, minor differences in polymer fraction can be accounted for.

6.3 Peel Strength

Peeling strength, also known as stripping strength was measured for freeze-thaw cycles $n \leq 7$. Values of peeling strength are only reported for cycle 2 and 3. All other cycles showed either cohesive failure tearing completely through one leg of the peeling specimen. 5 replicates were produced from 2 material batches for each freeze-thaw cycle. The detailed results of the testing are shown in Table 5.

Base layer cycle at overmold	Peeling Strength (kg/m)	Standard Deviation
1	Could not initiate peel	N/A
2	12.555	1.345
3	12.234	1.176
4	Bulk Failure	N/A
5	Bulk Failure	N/A
6	Bulk Failure	N/A
7	Bulk Failure	N/A

Table 5 – Peeling strength at various cycles, ASTM D903-98

Cycles 2 and 3 were the only base layer cycles, when overmolded to produce the peel sample, could be separated cleanly into two strips. All samples reported were immediately processed after injection of the top layer.

The regime of base layer conditions that produces separable bonds is unusual. Conventional thinking on bonding would suggest that the bond strength would trend up

with less crosslinking (lower cycle number) and with time, which was observed [53, 76, 77]. It was expected that another factor was contributing to the observed bond strength.

The PVA hydrogels under consideration are known to be macro porous [46, 47, 32]. It is thought the porosity of the PVA gels may promote the diffusion of an uncrosslinked solution through their surface. Hatakeyema, Uno, Yamada, Kishi and Hatakeyama have shown previously, using electron microscopy, that with increasing freeze thaw cycles the pore size increases and the pore wall thickens as the network densifies expelling bound water [78]. The pore size typically ranges from 10-100 μm , as described by various authors [62, 78, 50, 46].

6.4 Crystallinity

The crystallinity as determined by DSC has been reported by various authors to range from 0.5-7% of PVA [46, 61]. It has been noted that the endothermic peak observed is likely overlapped by the exothermic solvation of PVA in the presence of water. The superposition of these two simultaneous processes systematically underestimates the crystalline fraction when compared to other methods including x-ray diffraction and proton nuclear magnetic resonance imaging (H NMR) [61]. Due to complications caused by the presence of water in the samples, conclusions about the relationship between crystallinity and freeze thaw cycles could not be made. Values of crystalline fraction varied widely and artifacts in DSC heating curves made calculation a subjective exercise. A typical DSC heating curve after freeze-thaw cycle $n = 6$ is shown in.

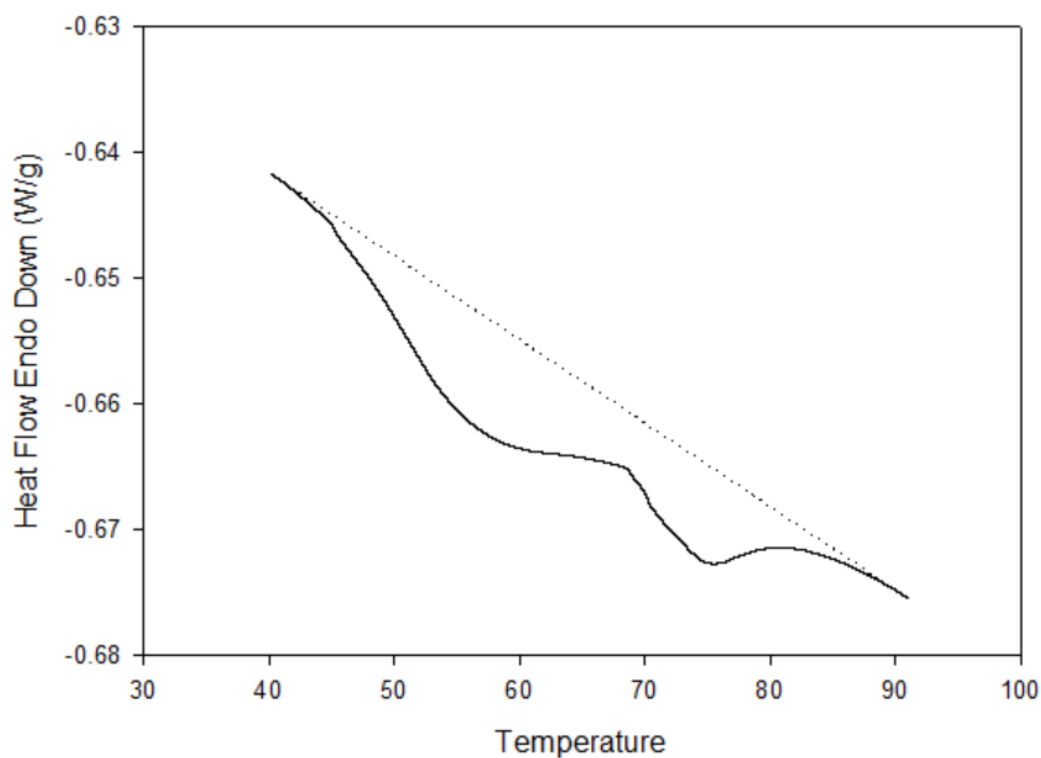


Figure 20 – Typical DSC heating curve for freeze-thaw cycle n=6 PVA hydrogel

Gel-solution transition occurred in the range of 40-90 °C for all cycles. The broad endothermic peak is generally shallower at lower numbers of freeze-thaw cycles. High water content (nominal 90 w%) and low degree of crystallinity, less than 10 % of the PVA network, means that crystalline fraction of the total sample weight is less than 1 % for all cycles. The measured value of crystallinity at freeze-thaw cycle n = 6 was determined by DSC to be 7.01 ± 0.45 w% of the PVA network. This is in agreement with the values reported in the literature. Other methods as described previously would be more appropriate for measurements of crystallinity.

The important finding from DSC heating curves is that PVA hydrogel based surgical models will remain stable below 40 °C. Surgical models are typically used at room temperature; however, it is feasible that they could be used at simulated human body temperature of 37 °C without significant changes in material properties [79].

6.5 Porosity

The porosity of the samples was inferred by the free water (non-freezable) following the methods of Plieva et al [62]. Free water volume is assumed to be the water that exists in the pores of the gel that is able to freeze because it is not bound in the swollen PVA network. To allow for comparisons between cycles the free water volume has been normalized to 10 w% PVA which corresponds to 8.54 v% PVA. The results of free water volume as determined by DSC measurements are shown in Figure 21. 3 replicates were measured for each cycle. The dashed line represents the total water volume in the sample, which includes both free and bound water.

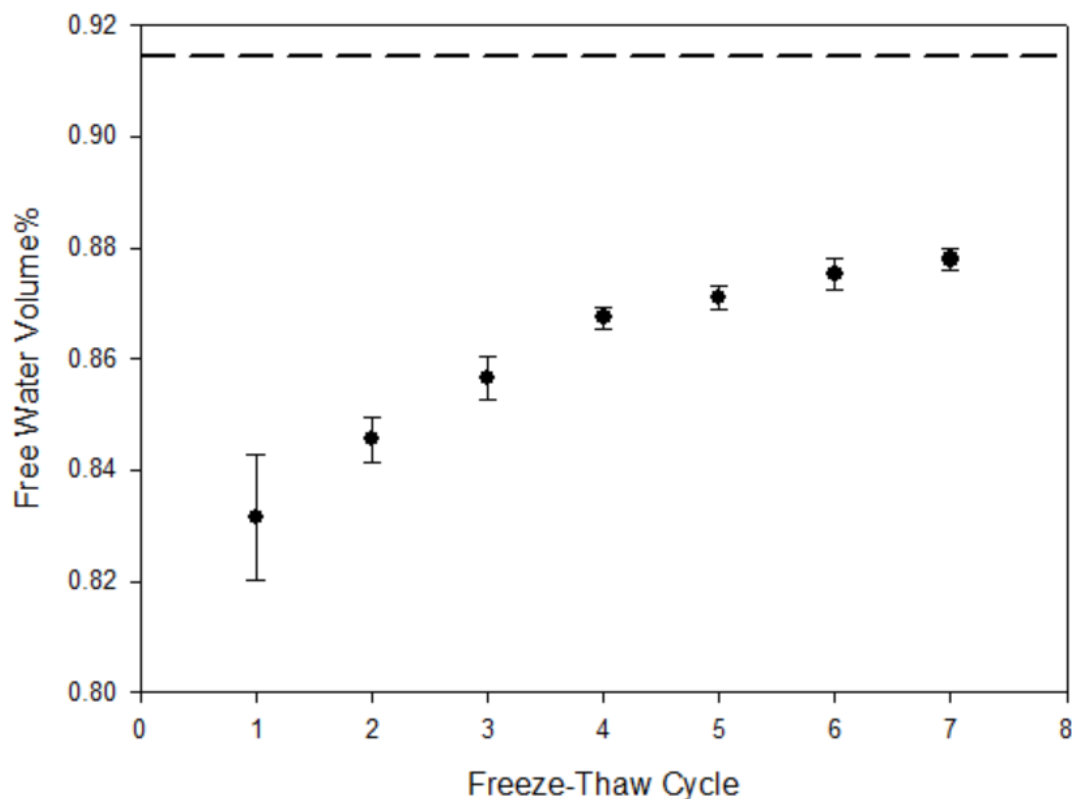


Figure 21 - Free water volume fraction with dashed horizontal line representing the total water volume in the sample.

The free water volume increases with each subsequent freeze thaw cycle. This indicates PVA network densification and decreased swelling in the polymer rich phase. As a consequence the pores become well defined as polymer chains are incorporated more densely into the network. Well-defined pores provide a less resistive path for diffusion across the interface, thus the water in the pores will become more dilute increasing the concentration gradient for diffusion.

The idea of macromolecular and small molecule diffusion in porous hydrogels has been investigated by various authors [80, 81, 82]. At the time of this study it seems that the

relationship between pore structure and diffusion of PVA solutions has not been investigated. It is likely that the macroscopic interconnected polymer pores of highly cycled PVA hydrogels provide a less resistive path for the diffusion of uncrosslinked PVA solution than the polymer rich phase of the network; however, this needs to be studied in detail.

The hydrodynamic radius of the PVA polymer chain of high molecular weight, as was used in this study, has been determined by dynamic light scattering to be of the order of 10nm [83, 84]. When pores are well defined at higher cycles, their large size (10-100 μ m) is not expected to hinder diffusion through the gel interface. This effect is thought to promote adhesion, which was observed at cycle $n=4$ and above.

6.6 Stability of PVA hydrogel

The dissolution of PVA when stored in deionized water was investigated for freeze-thaw cycles $n = 1-7$. The results of dissolution measurements are shown in Figure 22. 3 replicates were measured for each cycle and storage condition.

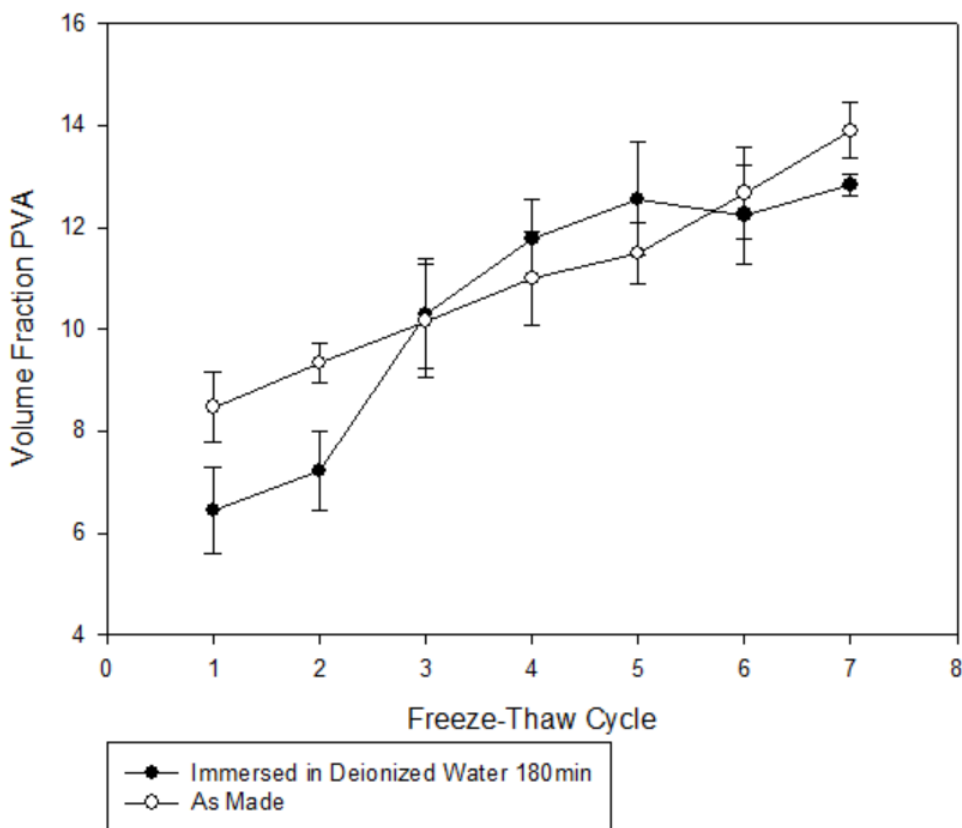


Figure 22 – PVA volume fraction comparison as-made and immersed in deionized water

After the first two freeze-thaw cycles, significant dissolution of PVA from the gels was observed. This is likely due to a combination of chains that are not tied to network junction points, and the solvation of small crystalline regions. The concept that PVA chains have greater mobility at lower freeze-thaw cycles, is reinforced by these observations.

It is not appropriate to draw a relationship between dissolution of PVA in deionized water and adhesion in overmolding. In overmolding, the gel is immersed in a medium of PVA solution. Measuring the dissolution in PVA solution was not attempted because the measurement would be complicated by PVA solution residue on the gels which would be

difficult to remove reliably. Furthermore, in overmolding the polymer poor phase of the gels would necessarily have a lower concentration of PVA than the overmolded solution. In such a situation, according to Fick's law of diffusion, the concentration gradient would have a driving force causing diffusion into the gel. When immersed in deionized water the opposite would occur; the driving force would cause diffusion of free PVA out from the gel.

6.7 Application of Controlled Adhesion

The investigation of peel strength led to the development of an embedded vessel model. The exact details of processing details have been omitted due to the commercialization of this model. The model consists of a vein (4 mm ID, 5 mm OD) embedded in a block of soft tissue with a 2.2 mm top layer representing the dermis layer of skin. Each component of the model has differing mechanical properties. The dermis layer is bonded strongly to the tissue block, while the embedded vein can be harvested from the tissue block. The embedded vessel model is shown in Figure 23.

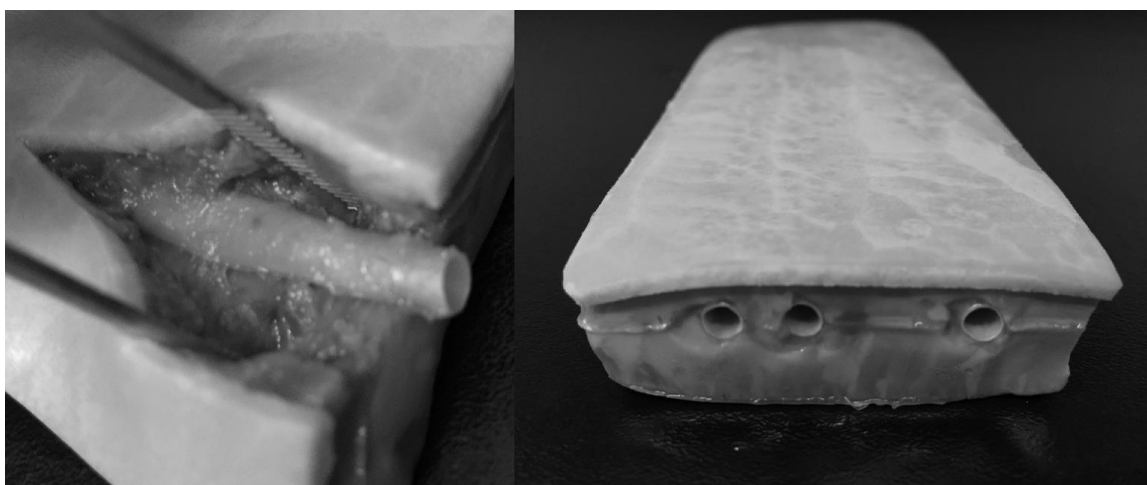


Figure 23 – Embedded vessel model (left) dissection of vein (right) cross section

The embedded vessel model was designed for the practice of vein harvesting for a variety of procedures. It has also been used with ultrasound imaging for practice needle insertion into veins and arteries. The differing densities of each component show distinct transitions in ultrasound imaging providing the same queues as natural tissue.

6.8 Rotational Molding

It was the objective to find the optimal thickener additional level that produced the most consistent part thickness. Initially three addition levels were used: 1, 3 and 5 parts per hundred (PPH) of PVA solution. The results of initial screening showed that 1 and 3 PPH could not hold a consistent wall thickness, whereas 5 PPH was too thick at molding temperature to flow and disperse in the mold cavity. A defective under-filled part is shown in Figure 24.

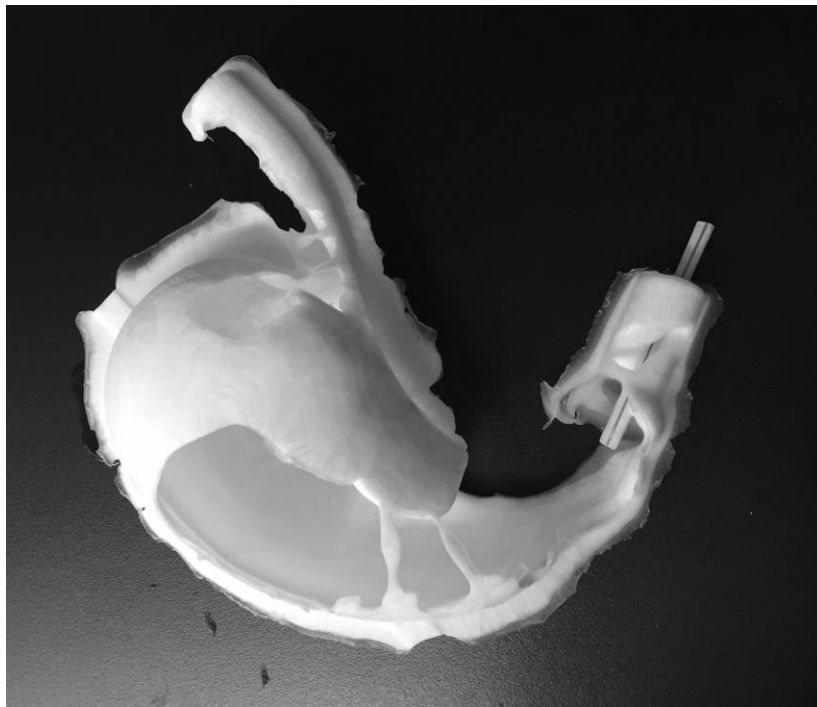


Figure 24 – Stomach 5 PPH Fumed Silica 10 w% PVA, under filled (frozen)

When the thickened PVA solution is too thick at room molding temperatures the mold does not completely fill. When the thickened PVA solution is too thin the mold fills; however, on cooling to room temperature is not able to support the wall thickness. A balance between flow at molding temperature and stability at room temperature is needed.

With poor results from all addition levels in the initial screening a heuristic approach was employed to find an acceptable level. At 4 PPH thinning was still observed in the demolded part. Both 4.5 and 4.25 PPH were examined and it was determined that 4.25 PPH of fumed silica produced the most consistent wall thickness with full mold coverage. The resulting demolded part after freeze-thaw cycle $n = 3$ is shown in Figure 25.

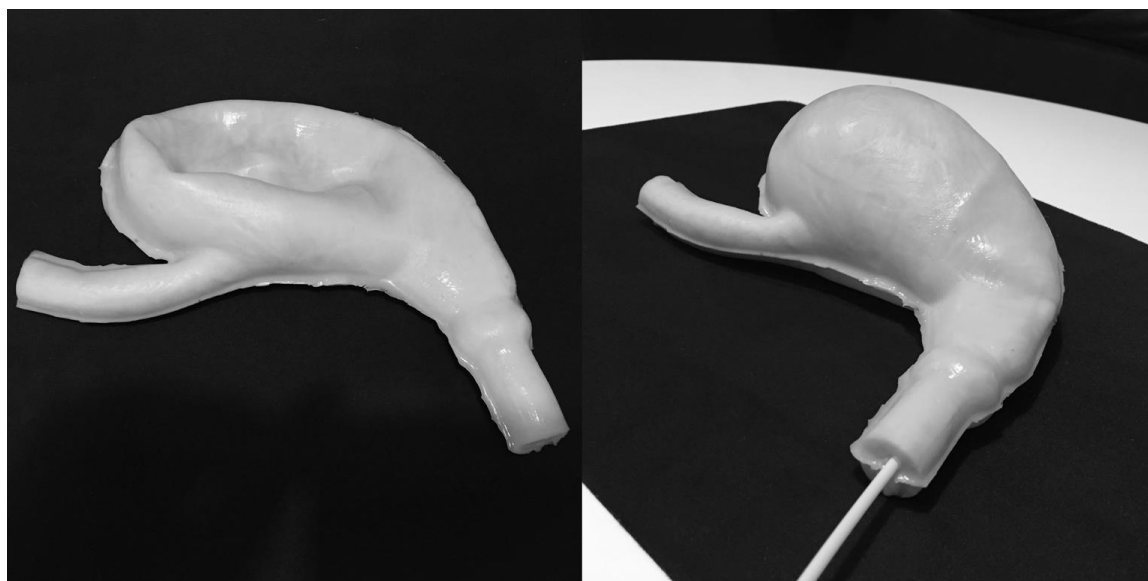


Figure 25 – Stomach model 4.25 PPH fumed silica, 10w% PVA. (left) Stomach as made (right) stomach in expanded state.

6.8.1 Thickener Effect on Elastic Modulus

Fumed silica addition levels were significant relative to the PVA fraction in the rotomolding material system. On a volume basis, the ratio of PVA to fumed silica was 4.1, which produced the desired molding results.

In order to characterize the effect of fumed silica on the resulting gel stiffness, tensile testing was done on 10 wt% PVA solution and on the same solution with thickener addition. Tensile results were collected at cycles 3 and 6, the results are shown in Figure 26. 5 replicates were measured for each cycle and material.

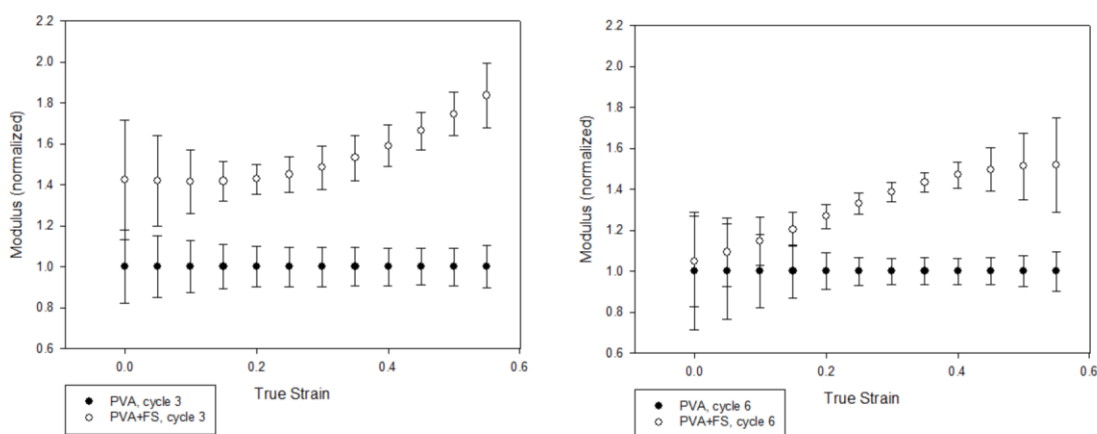


Figure 26 – Modulus of fumed silica thickened PVA hydrogel normalized to control PVA without thickener addition. (Left) 3rd freeze-thaw cycle (right) 6th freeze-thaw cycle.

The results of tensile testing showed a clear effect on the modulus of the thickened PVA gel material. In general, the relative difference in modulus is greater at higher strains. For cycle $n = 6$, at low strains the relative difference is likely not significant. On handling the gels is unlikely that users would be able to perceive the difference. However, the intended

procedures for this model include the use of medical staplers that may be sensitive to the material elastic modulus. In order to match the elastic modulus of non-thickened PVA materials it may be necessary to process thickened PVA at a lower number of freeze-thaw cycles.

6.8.2 Thickener Effect on Residual Stress

When conditioning samples for tensile testing, it was noticed that the samples containing fumed silica behaved differently than those without. Relief on the residual stress in samples during conditioning can be visualized in the first loading-unloading curve of a tensile test. A hysteresis loop is always present on the first loading of PVA materials due to residual stress in the material that requires work to relieve. The hysteresis curves for the first loading-unloading cycle of both thickened and non-thickened PVA are shown in Figure 27.

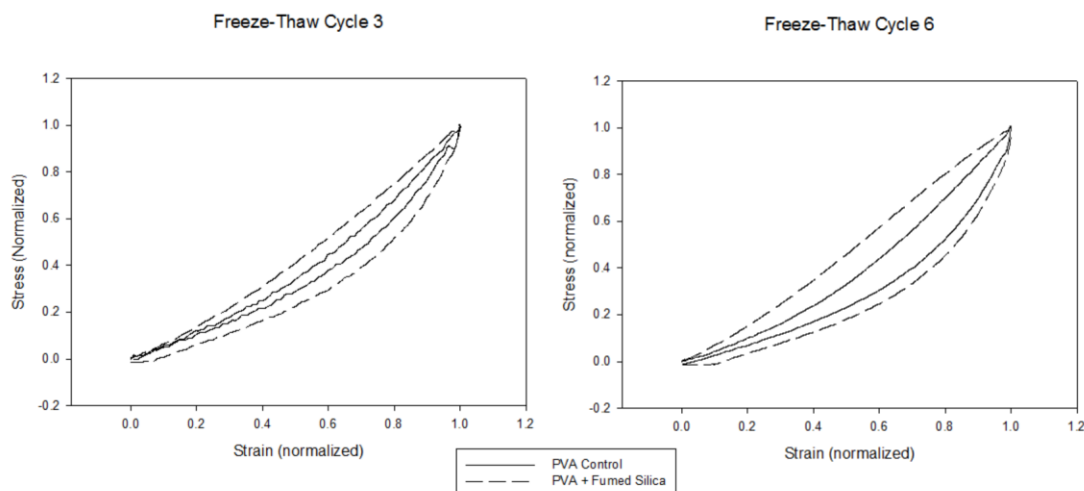


Figure 27 – Typical normalized hysteresis curves for non-thickened and thickened PVA during first load-unload cycle in tension. (left) freeze-thaw cycle 3 (right) freeze-thaw cycle 6.

Subsequent loading cycles do not exhibit the hysteresis loop observed on the first loading cycle. This indicates that at the strain rate used there is not significant losses from viscoelasticity and the hysteresis loop observed on the first cycle is mainly due to irreversible changes in the material during preconditioning of the samples. Furthermore, the area in the hysteresis loop is larger than that of the control samples. This is likely due to network formation of fumed silica which causes the thickening action seen in the liquid solution. The modulus of the fumed silica thickened PVA material will appear higher on a first loading than it will after conditioning.

6.9 Summary

This study investigated joining methods of PVA hydrogels and the properties that influence bond strength. Also, molding techniques were investigated to create complex models. A

method of sample preparation for peel strength specimens was created. A method of creating thin walled hollow structures using rotational molding was also developed.

Tensile testing showed that changes in the PVA network plateau after freeze-thaw cycle $n = 7$. The measured elastic modulus was found to increase beyond the seventh cycle however this was attributed to loss of water which effectively increased the polymer fraction of the samples. Tensile data was normalized to a 10 w% PVA to correct to differences in water content of the specimens.

Peel strength

An unusual relationship was observed during peel strength testing. At freeze-thaw cycle $n = 1$ strong bonding was observed with the samples being inseparable. Freeze-thaw cycles $n = 2-3$ peeled smoothly during testing with 12.5 ± 1.34 kg/m and 12.23 ± 1.18 kg/m respectively. For freeze-thaw cycles $n \geq 3$, strong bonding was observed with failure in the bulk material during testing. The macroscopic porosity of the samples was determined by DSC measurements of free water in the samples. For PVA specimens containing 88.3 v% water, the free water volume fraction increased from 83.1 ± 1.1 v% to 87.8 ± 0.2 v%. Dissolution measurements showed that significant polymer was lost from PVA specimens stored in deionized water for freeze-thaw cycles $n = 1-2$ indicating high mobility of polymer chains in the network. Strong bonding was attributed to low degree of crosslinking for freeze-thaw cycle $n = 1$ and to well defined pores which allow interfacial diffusion for freeze-thaw cycles $n \geq 3$. Smooth peeling for freeze-thaw cycles $n = 2-3$ was attributed to sufficient crosslinking and insufficient porosity to form a strong bond during overmolding.

Rotational molding for hollow structures

Rotational molding was investigated as a method to produce complex hollow structures. It was found that addition of fumed silica to PVA solution produced a viscous paste with thixotropic properties. At elevated temperatures the paste could be distributed evenly onto the wall of a mold and upon cooling would hold a stable wall thickness which could be further crosslinked physically into a hydrogel. Through heuristic selection of thickener levels it was determined that 4.25 parts per hundred of PVA solution created a stable 3 mm wall thickness. The elastic modulus of the thickened PVA gel was compared to the base material. The elastic modulus of thickened PVA was in general greater than PVA alone. At freeze-thaw cycle $n = 3$ the elastic modulus of fumed silica thickened PVA was found to be 183 ± 16 % greater PVA alone at a true strain of 0.55. The effect on the modulus decreased both with the strain at which the modulus was measured and with increasing freeze-thaw cycles.

Chapter 7

7 Conclusions

The objectives of this study were to investigate joining methods and molding techniques for the production of complex surgical training models. The following conclusions were made with respect to these objectives.

- The polymer fraction PVA hydrogels increases with the number of freeze-thaw cycles due to loss of water.
- Bond strength of overmolded PVA hydrogels is related to both the degree of crosslinking and porosity in the base layer.
- A regime of cycles exists at freeze-thaw cycles $n = 2-3$ where peeling occurs adhesively.
- With increasing freeze-thaw cycles the network of PVA hydrogels densifies, expelling bound water from the network and increasing porosity.
- At freeze-thaw cycles $n = 1-2$ PVA hydrogel are not stable when stored in deionized water and significant polymer is lost from the gel.
- Fumed silica is used as a thickening agent for PVA solution to create a thixotropic gel capable of being rotationally molded. The production of a hollow stomach model was produced in this manner.
- The addition of fumed silica causes a significant increase in the elastic modulus. The effect on elastic modulus proportionally larger at higher strains.

Chapter 8

8 Future Applications and Outlook

8.1 Introduction

PVA hydrogels are a useful material in many applications and it was the goal of this work to investigate the processing methods for the joining, characterize the strength of adhesion between joined materials, and the production of complex surgical training models. Future work would involve developing new techniques for the production of complex models, as well as improving the efficiency of existing methods.

The development of surgical training models is often an iterative process. There is a need for rapid prototyping to accelerate and reduce the costs associated with the development cycle. 3D printing is a potential technology for the rapid production of surgical model prototypes. Fused deposition modeling of PVA hydrogels by physical and chemical crosslinking is an area of interest for future developments.

The models in this work incorporated homogenous PVA hydrogels. In models such as lung and kidney the internal structure is non-uniform. Incorporating the findings of this study on the production of hollow structures with materials mimicking the internal structures of organs is an area for future development.

Joining methods investigated in this study produced strong bonds. However, when PVA was used as an adhesive the time-scale of bond formation is at least the length of a freeze-thaw cycle. When cyanoacrylate based adhesives were used instant bonds were formed but

they were brittle and dissimilar from the bulk material. Ideally an adhesive could be found that rapidly bonds PVA hydrogel while producing a bond that had similar properties to the surrounding material. Investigation of instant adhesive compound that polymerize in the presence of water would be advantageous for the rapid production of complex models. PVA may be appropriate in critical areas whereas instant adhesives would be useful in non-critical applications.

9 References

- [1] Royal College of Physicians and Surgeons of Canada, "Accredited RCPSC Programs," 11 June 2015. [Online]. Available: http://www.royalcollege.ca/portal/page/portal/rc/common/documents/accreditation/accredited_rcpsc_programs_e.pdf.
- [2] Schulich School of Medicine and Dentistry, "General Surgery Curriculum," [Online]. Available: <https://www.schulich.uwo.ca/generalsurgery/docs/Curriculum.pdf>.
- [3] E. M. Webber and K. A. Harris, "The Future of General Surgery: Evolving to meet a changing practice," Royal College of Physicians and surgeons of Canada, 2014.
- [4] P. Santoni-Rugiu and P. J. Sykes, *A History of Plastic Surgery*, Heidelberg: Springer-Verlag Berlin, 2007.
- [5] E. H. Akerknecht, "From Barber-Surgeon to Modern Doctor," *Bulletin of the History of Medicine*, pp. 545-53, Winter 1984.
- [6] J. L. Cameron, "William Stewart Halsted," *Annals of Surgery*, vol. 225, no. 5, pp. 445-458, 1997.
- [7] A. S. S. Thomsen, Y. Subhi, J. F. Killgaard, M. La Cour and L. Konge, "Update on Simulation-Based Surgical Training and Assessment in Ophthalmology," *American Academy of Ophthalmology*, vol. 122, no. 6, pp. 1111-1130, 2015.
- [8] R. Aggarwal et al., "Training and simulation for patient safety," *BMJ Quality and Safety*, vol. 19, no. Suppl 2, pp. i34-i43, 2010.
- [9] G. A. Ewy et al., "Test of a cardiology patient simulator with students in fourth-year electives," *Journal of Medical Education*, vol. 62, no. 9, pp. 738-43, 1987.
- [10] Goshen College, "Fetal Pig Dissection Guide Human/Pig Comparisons," [Online]. Available: <https://www.goshen.edu/bio/pigbook/humanpigcomparison.html>. [Accessed 16 February 2016].
- [11] Academy of Surgical Research, "Guidelines for Training in Surgical Research with Animals," *Journal of Investigative Surgery*, vol. 22, pp. 218-225, 2009.
- [12] A. Parra-Blanco, N. González, R. González, J. Ortiz-Fernández-Sordo and C. Ordieres, "Animal Models for Endoscopic Training: Do we Really Need Them?," *Endoscopy*, vol. 45, no. 06, pp. 478-484, 2013.

- [13] P. H. Cosman, P. C. Cregan, C. J. Martin and J. A. Cartmill, "Virtual reality simulators: Current status in acquisition and assessment of surgical skills," *ANZ Journal of Surgery*, vol. 72, no. 1, pp. 30-34, 2002.
- [14] M. Silvennoinen, S. Helfenstein, M. Ruoranen and P. Saariluoma, "Learning basic surgical skills through simulator training," *Instructional Science*, vol. 40, no. 5, pp. 769-783, 2012.
- [15] University of Southern California, "What is laparoscopic surgery," 2002. [Online]. Available:
<http://www.surgery.usc.edu/divisions/tumor/pancreasdiseases/web%20pages/laparoscopic%20surgery/WHAT%20IS%20LAP%20SURGERY.html>. [Accessed 18 February 2016].
- [16] 3-Dmed, "Minimally Invasive Training System (MITS) SERIES," 2016. [Online]. Available: <https://www.3-dmed.com/product/minimally-invasive-training-system-mits-series>. [Accessed 18 February 2016].
- [17] EoSurgical, "EoSim for Institutions," 2016. [Online]. Available:
<http://www.eosurgical.com/collections/simulators-institutions>. [Accessed 18 February 2016].
- [18] Encoris, "Surgical Training Models," 2016. [Online]. Available:
<http://www.encoris.com/surgical-training-models/>. [Accessed 18 February 2016].
- [19] SimuLab, "Product," 2016. [Online]. Available:
<https://www.simulab.com/products>. [Accessed 18 February 2016].
- [20] Sawbones, "Surgical Models," 2016. [Online]. Available:
<http://www.sawbones.com/Catalog/Surgical%20Models>. [Accessed 18 February 2016].
- [21] Smooth-On, "Medical Simulation," 2016. [Online]. Available: <http://www.smooth-on.com/Medical-Simulation/c1425/index.html>. [Accessed 18 February 2016].
- [22] O. Wichterle and D. Lim, "Hydrophilic gels for biological use," *Nature*, vol. 185, no. 4706, p. 117-118, 1960.
- [23] M. Cavagnaro, F. Frezza, R. Laurita and M. Tannino, "A model to evaluate dielectric properties of human tissues based on water content," in *International Symposium on Medical Information and Communication Technology*, Florence, 2014.

- [24] M. L. Fackler and J. A. Malinowski, "Ordnance gelatin for ballistic studies. Detrimental effect of excess heat used in gelatin preparation," *The American journal of forensic medicine and pathology*, vol. 9, no. 3, pp. 218-219, 1988.
- [25] T. F. Juliano et al., "Multiscale mechanical characterization of biomimetic physically associating gels," *Journal of Materials Research*, vol. 21, no. 8, pp. 2084-2092, 2006.
- [26] J.-Y. Sun et al., "Highly stretchable and tough hydrogels," *Nature*, vol. 489, no. 7414, pp. 133-136, 2012.
- [27] J. P. Gong, "Why are double network hydrogels so tough?," *Soft Matter*, vol. 6, no. 12, pp. 2583-2590, 2010.
- [28] Encyclopædia Britannica, "Polyvinyl alcohol (PVA) Chemical compound," 2016. [Online]. Available: <http://www.britannica.com/science/polyvinyl-alcohol>. [Accessed 20 February 2016].
- [29] Sekisui, "Solution Preparation Guidelines," [Online]. Available: http://www.sekisui-sc.com/wp-content/uploads/SelvolPVOH_SolutionPreparationGuidelines_EN.pdf. [Accessed 20 February 2016].
- [30] Kuraray, "Technical Information - aqueous solution of PVA," 2004. [Online]. Available: http://www.poval.jp/english/poval/tec_info/ti_02.html. [Accessed 20 February 2016].
- [31] T. Itou, H. Kitai, A. Shimazu, T. Miyazaki and K. Tashiro, "Clarification of cross-linkage structure in boric acid doped poly(vinyl alcohol) and its model compound as studied by an organized combination of X-ray single-crystal structure analysis, Raman spectroscopy, and density functional theoretical calculation," *The journal of physical chemistry*, vol. 118, no. 22, p. 6032-6037, 2014.
- [32] C. M. Hassan and N. A. Peppas, "Structure and Applications of Poly(vinyl alcohol) Hydrogels Produced by Conventional Crosslinking or by Freezing/Thawing Methods," *Advances in Polymer Science*, vol. 153, pp. 37-65, 2000.
- [33] J. M. Gohil, A. Bhattacharya and P. Ray, "Studies on the Cross-linking of Poly(Vinyl Alcohol)," *Journal of Polymer Research*, vol. 14, no. 2, pp. 161-169, 2006.
- [34] T. Tanabe and M. Nambu, "Medical material of polyvinyl alcohol and process of making". United States Patent US4734097, 29 March 1988.

- [35] N. Peppas, "Turbidimetric studies of aqueous poly(vinyl alcohol) solutions," *Macromolecular Chemistry and Physics*, vol. 176, no. 11, p. 3433–3440, 1975.
- [36] S. P. Papkov and A. K. Dibrova, "Spontaneous Gelation of Polymer Solutions," *Polymer Science U.S.S.R.*, vol. 25, no. 3, pp. 741-747, 1981.
- [37] W. L. Wu, M. Shibayama, S. Roy, H. Kurokawa, L. D. Coyne, S. Nomura and R. S. Stein, "Physical gels of aqueous poly(vinyl alcohol) solutions: a small-angle neutron-scattering study," *Macromolecules*, vol. 23, no. 8, p. 2245–2251, 1990.
- [38] K. Ogasawara, T. Nakajima, K. Yamaura and S. Matsuzawa, "Effect of syndiotacticity on the aqueous poly(vinyl alcohol) gel 2. Syneresis of gel," *Colloid and Polymer Science*, vol. 254, no. 5, pp. 456-461, 1976.
- [39] M. Djabourov, K. Nishinari and S. B. Ross-Murphy, "Gelation through phase transformation," in *Physical Gels from Biological and Synthetic Polymers*, Cambridge University Press, 2013, pp. 222-255.
- [40] Sekisui, "A Versatile High Performance Polymer," 2016. [Online]. Available: http://www.sekisui-sc.com/wp-content/uploads/SelvolPVOH_Brochure_EN.pdf. [Accessed 20 February 2016].
- [41] L. Domotenko, V. Lozinskii, Y. Vainerman and S. Rogozhin, "Effect of freezing conditions of dilute solutions of polyvinyl alcohol and conditions of defreezing samples on properties of cryogels obtained," *Polymer Science U.S.S.R.*, vol. 30, no. 8, pp. 1758-1764, 1988.
- [42] V. I. Lozinsky, L. G. Damshkaln, I. N. Kurochkin and I. I. Kurochkin, " Study of cryostructuring of polymer systems. 33. Effect of rate of chilling aqueous poly(vinyl alcohol) solutions during their freezing on physicochemical properties and porous structure of resulting cryogels," *Colloid Journal*, vol. 74, no. 3, pp. 319-327, 2012.
- [43] V. I. Lozinsky, A. L. Zubov, I. N. Savina and P.M. Fatima, "Study of cryostructuring of polymer systems. XIV. Poly(vinyl alcohol) cryogels: Apparent yield of the freeze–thaw-induced gelation of concentrated aqueous solutions of the polymer," *Journal of Applied Polymer Science*, vol. 77, no. 8, pp. 1822-1831, 2000.
- [44] W. K. Wan, G. Campbell, Z. F. Zhang, A. J. Hui and D. R. Boughner, "Optimizing the tensile properties of polyvinyl alcohol hydrogel for the construction of a bioprosthetic heart valve stent," *Journal of Biomedical Materials Research*, vol. 63, no. 6, p. 854–861, 2002.

- [45] M. Lisa Brannon and Nikolaos A. Peppas, "Solute diffusion in swollen membranes," *Journal of Membrane Science*, vol. 32, no. 2, pp. 125-138, 1987.
- [46] P. J. Willcox et al., "Microstructure of Poly(vinyl alcohol) Hydrogels Produced," *Journal of Polymer Science Part B: Polymer Physics*, vol. 37, no. 24, pp. 3438-3454, 1999.
- [47] F. M. Plieva and et al., "Pore Structure of Macroporous Monolithic Cryogels," *Journal of Applied Polymer Science*, vol. 100, no. 2, pp. 1057-1066, 2006.
- [48] R. Ricciardi and et al., "Structural Organization of Poly(vinyl alcohol) Hydrogels Obtained," *Chemistry of Materials*, vol. 17, no. 5, pp. 1183-1189, 2005.
- [49] J. A. Stammen, S. Williams, D. N. Ku and R. E. Guldberg, "Mechanical properties of a novel PVA hydrogel in shear and unconfined compression," *Biomaterials*, vol. 22, no. 8, p. 799-806, 2001.
- [50] L. E. Millon, M.-P. Nieh, J. L. Hutter and W. Wan, "SANS Characterization of an Anisotropic Poly(vinyl alcohol) Hydrogel with Vascular Applications," *Macromolecules*, vol. 40, no. 10, pp. 3655-3662, 2007.
- [51] S. Standring, *Gray's Anatomy the Anatomical Basis of Clinical Practice*, Churchill Livingstone, 2005.
- [52] D. G. King, "Connective Tissue Study Guide," SIU School of Medicine, 2015 April 2015. [Online]. Available: <http://www.siumed.edu/~dking2/intro/ct.htm#ordinspecial>. [Accessed 21 February 2016].
- [53] N. Maeda, N. Chen, M. Tirrell and J. N. Israelachvili, "Adhesion and Friction Mechanisms of Polymer-on-Polymer Surfaces," *Science*, vol. 297, no. 5580, pp. 379-382, 2002.
- [54] A. Phadke and et al., "Rapid self-healing hydrogels," *Proceedings of the National Academy of Sciences of the United States of America*, vol. 109, no. 12, pp. 4383-4388, 2012.
- [55] R. Carlsen and R. Joannou, "Roto 101," Association of Rotational Molders, April 2013. [Online]. Available: <http://www.rotomolding.org/About/Roto101.aspx>. [Accessed 21 February 2016].
- [56] L. E. Millon and W. K. Wan, "The polyvinyl alcohol-bacterial cellulose system as a new nanocomposite for biomedical applications," *Journal of Biomedical*

Materials Research Part B: Applied Biomaterials, vol. 79B, no. 2, p. 245–253, 2006.

- [57] Olfa, "OLFA® Splash 45mm Rotary Cutter, Aqua (RTY-2/C)," 2016. [Online]. Available: <http://www.olfa.com/splash-45mm-rotary-cutter%2C-aqua-%28rty-2%2Fc%29/1110720.html#start=4>. [Accessed 26 February 2016].
- [58] ASTM International, *Standard Test Method for Peel or Stripping Strength of Adhesive Bonds*, West Conshohocken, PA, 2010.
- [59] Henkel, "Technical Data Sheet Loctite 495," 2016. [Online]. Available: http://www.loctite.sg/sea/content_data/93801_495EN.pdf. [Accessed 28 February 2016].
- [60] 3M, "Understanding Adhesion," 2016. [Online]. Available: http://www.3m.com/US/mfg_industrial/MAP/3M_IATD_SEMINAR/Understanding_Adhesion/8.1.2.html. [Accessed 29 February 2016].
- [61] R. Ricciardi, F. Auriemma, C. Gaillet and C. De Rosa, "Investigation of the Crystallinity of Freeze/Thaw Poly(vinyl alcohol) Hydrogels by Different Techniques," *Macromolecules*, vol. 37, no. 25, pp. 9510–9516, 2004.
- [62] F. Plieva et al., "Pore structure of macroporous monolithic cryogels prepared from poly(vinyl alcohol)," *Journal of Applied Polymer Science*, vol. 100, no. 2, p. 1057–1066, 2006.
- [63] G. Höhne, W. Hemminger and H. J. Flammersheim, *Differential scanning calorimetry: an introduction for practitioners*, Berlin, New York: Springer-Verlag, 1996.
- [64] C. M. Hassan, J. H. Ward and N. A. Peppas, "Modeling of crystal dissolution of poly(vinyl alcohol) gels produced by freezing/thawing processes," *Polymer*, vol. 41, no. 18, p. 6729–6739, 2000.
- [65] C. E. Macias, H. Bodugoz-Senturk and O. K. Muratoglu, "Quantification of PVA hydrogel dissolution in water and bovine serum," *Polymer*, vol. 54, no. 2, pp. 724–729, 2013.
- [66] G. Beall, *Rotational Molding*, Cincinnati: Hanser/Gardner Publications, 1998.
- [67] Advantage Plastics, "Thermoforming Materials," [Online]. Available: <http://www.advplasticsny.com/materials.html>. [Accessed 29 February 2016].

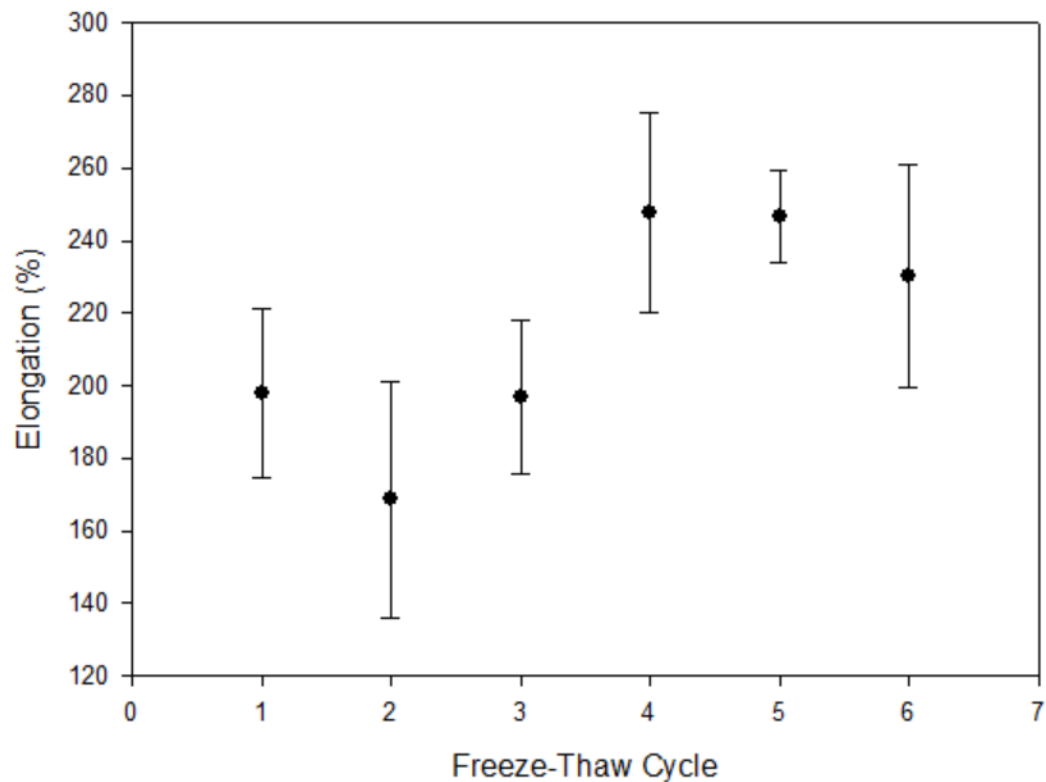
- [68] A. Csendes and A. M. Burgos, "Size, Volume and Weight of the Stomach in Patients with Morbid Obesity Compared to Controls," *Obesity Surgery*, vol. 15, no. 8, pp. 1133-1136, 2005.
- [69] H. Elariny, H. González and B. Wang, "Tissue Thickness of Human Stomach Measured on Excised Gastric Specimens from Obese Patients," *Surgical Technology International*, vol. 14, pp. 119-124, 2005.
- [70] H. J. Kwon and A. D. Rogalsky, "Mechanical characterisation of hydrogel," *Society of Plastics Engineers*, 2010.
- [71] M. A. Haque, T. Kurokawa and J. P. Gong, "Super tough double network hydrogels and their application as biomaterials," *Polymer*, vol. 53, no. 9, pp. 1805-1822, 2012.
- [72] A. Karimi, M. Navidbakhsh, H. Yousefi and M. Alizadeh, "An experimental study on the elastic modulus of gelatin hydrogels using different stress-strain definitions," *Journal of Thermoplastic Composite Materials*, vol. 28, no. 10, pp. e3-e4, 2014.
- [73] J. H. Lee and et al., "A Novel Method for the Accurate Evaluation of Poisson's Ratio of Soft Polymer Materials," *The Scientific World Journal*, vol. 2013, 2013.
- [74] G. Box, J. Hunter and W. Hunter, *Statistics for Experimenters*, Hoboken, New Jersey: John Wiley & Sons, 2005.
- [75] N. A. Peppas and E. W. Merrill, "Differential scanning calorimetry of crystallized PVA hydrogels," *Journal of Applied Polymer Science*, vol. 20, no. 6, pp. 1457-1465, 1976.
- [76] M. A. Ansarifar, K. N. G. Fuller and G. J. Lake, "Adhesion of Unvulcanized Elastomers," *International Journal of Adhesion and Adhesives*, vol. 13, no. 2, pp. 105-110, 1993.
- [77] A. N. Gent, "The role of chemical bonding in adhesion of elastomers," *International Journal of Adhesion and Adhesives*, vol. 4, no. 1, pp. 175-180, 1981.
- [78] T. Hatakeyema, J. Uno, C. Yamada, A. Kishi and H. Hatakeyama, "Gel-sol transition of poly(vinyl alcohol) hydrogels formed by freezing and thawing," *Thermochimica Acta*, vol. 431, no. 1, pp. 144-148, 2005.
- [79] WebMD, "Body Temperature," 14 November 2014. [Online]. Available: <http://www.webmd.com/first-aid/body-temperature>.

- [80] M. J. Gordon, K. C. Chu, A. Margaritis, A. J. Martin, C. R. Ethier and B. K. Rutt, "Gordon, M J; Chu, K C; Margaritis, A; Martin, A J; Ethier, C R; Rutt, B K," *Biotechnology and bioengineering*, vol. 65, no. 4, pp. 459-467, 1999.
- [81] A. Michelman-Ribeiro, H. Boukari, R. Nossal and F. Horkay, "Fluorescence Correlation Spectroscopy Study of Probe Diffusion in Poly(Vinyl Alcohol) Solutions and Gels," *Fluorescence Correlation Spectroscopy Study of Probe Diffusion in Poly(Vinyl Alcohol) Solutions and Gels*, vol. 227, no. 1, pp. 221-230, 2005.
- [82] A. Pluen, P. A. Netti, R. K. Jain and D. A. Berk, "Diffusion of Macromolecules in Agarose Gels: Comparison of Linear and Globular Configurations," *Biophysical Journal*, vol. 77, no. 1, p. 542-552, 1999.
- [83] Y. Jiang, "Poly(vinyl alcohol) for Biomedical Applications," 2009.
- [84] B. Wang, S. Mukataka, M. Kodama and E. Kokufuta, "Viscometric and Light Scattering Studies on Microgel Formation by γ -Ray Irradiation to Aqueous Oxygen-free Solutions of Poly(vinyl alcohol)," *Langmuir*, vol. 12, no. 23, pp. 6108-6114, 1997.
- [85] K. Haraguchi, K. Uyama and H. Tanimoto, "Self-healing in Nanocomposite Hydrogels," *Macromolecular rapid communications*, vol. 32, no. 16, p. 1253-1258, 2011.
- [86] L. E. Millon, "Isotropic and anisotropic polyvinyl alcohol based hydrogels for biomedical applications (Doctoral Dissertation)," *London, Ont. : Faculty of Graduate Studies, University of Western Ontario*, 2006.
- [87] D. R. Lide, *CRC Handbook of Chemistry and Physics: A Ready-reference Book of Chemical and Physical Data*, Boca Raton: CRC Press, 1995.
- [88] J. E. Mark, *Physical Properties of Polymers Handbook*, Woodbury, NY: American Institute of Physics, 1998.
- [89] K. E. Roberts, R. L. Bell and A. J. Duffy, "Evolution of Surgical Training," *World Journal of Gastroenterology*, vol. 12, no. 20, pp. 3219-3224, 2006.

Appendices

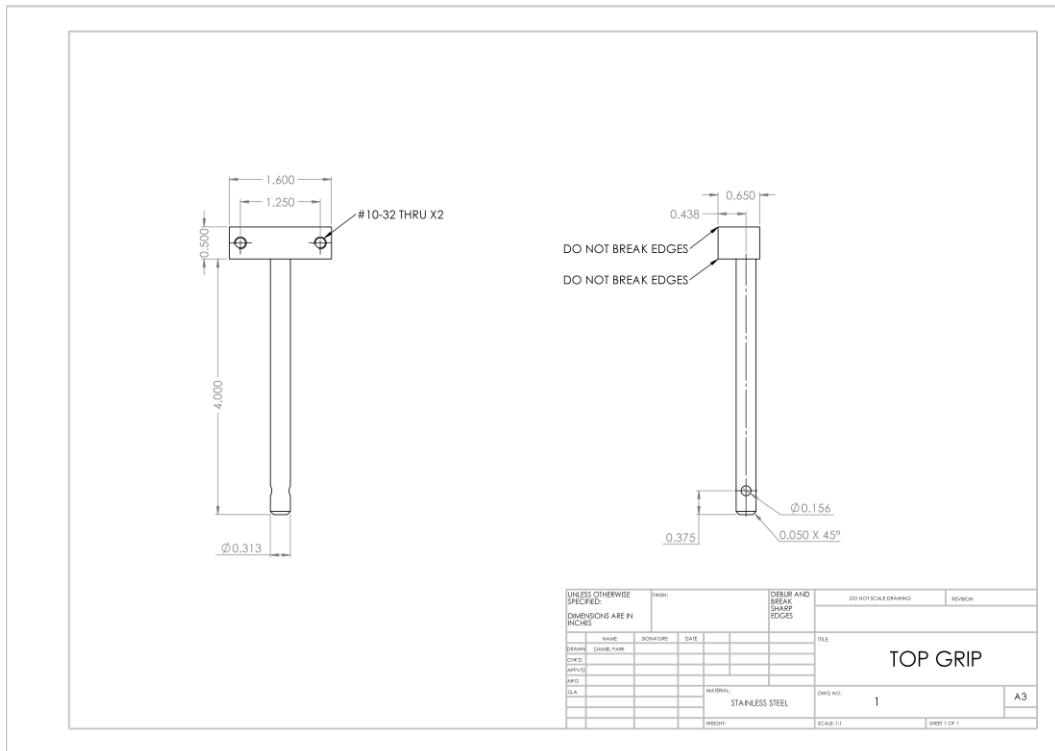
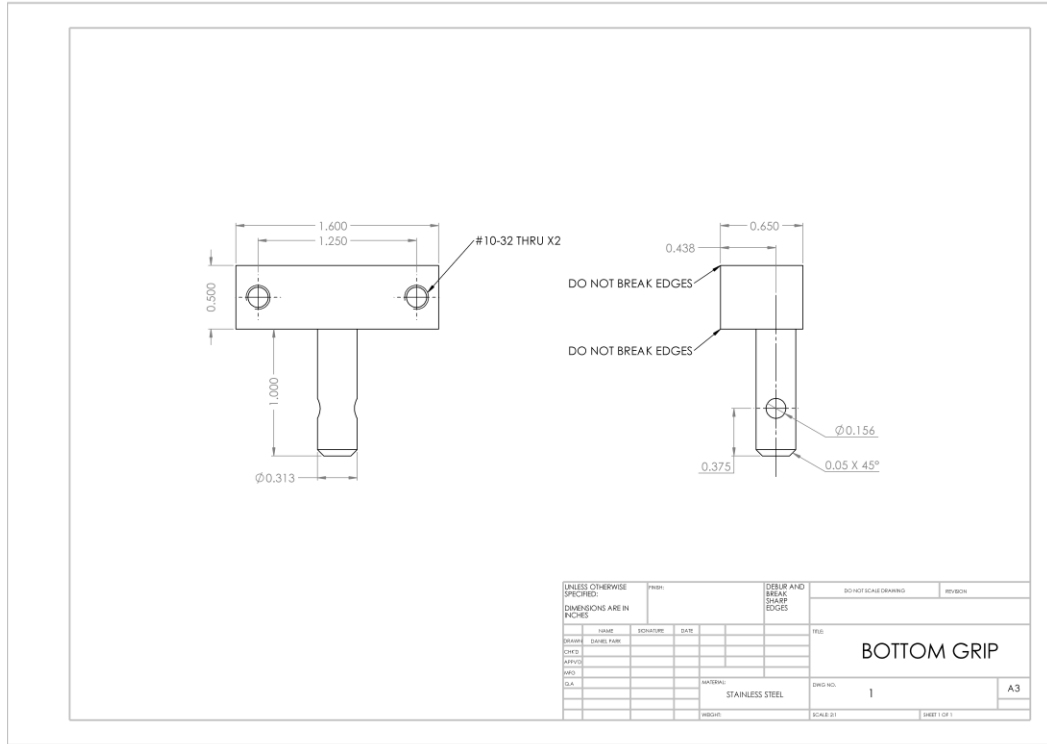
Appendix A: Ring Extensometry

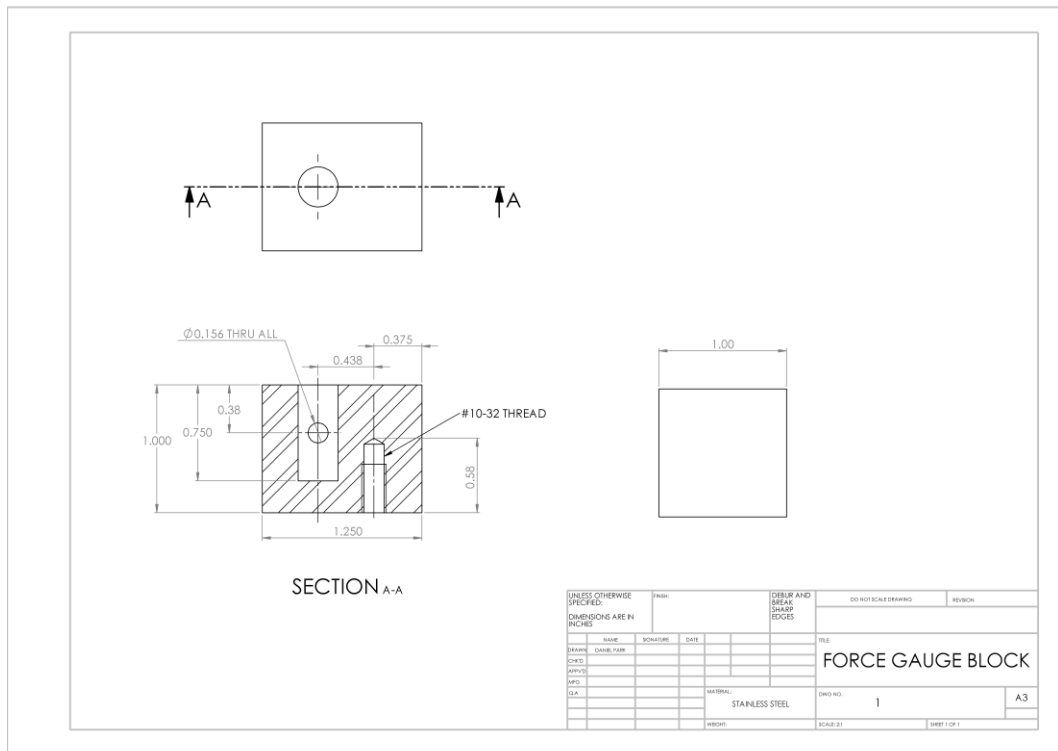
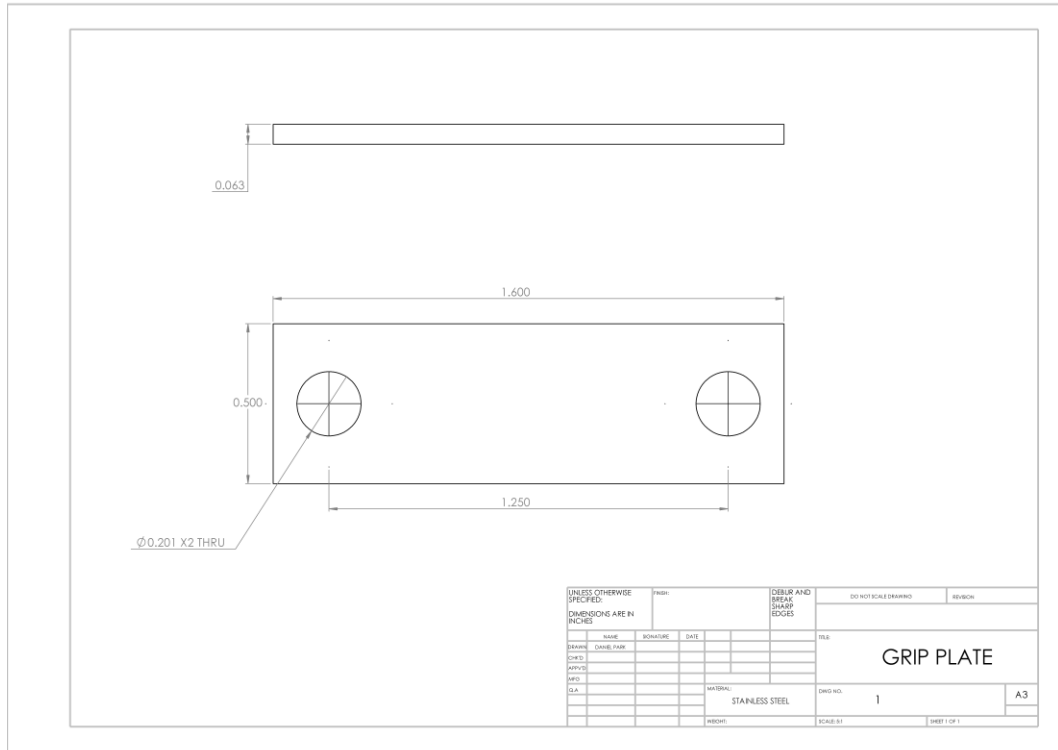
ASTM D412 – Test Method B

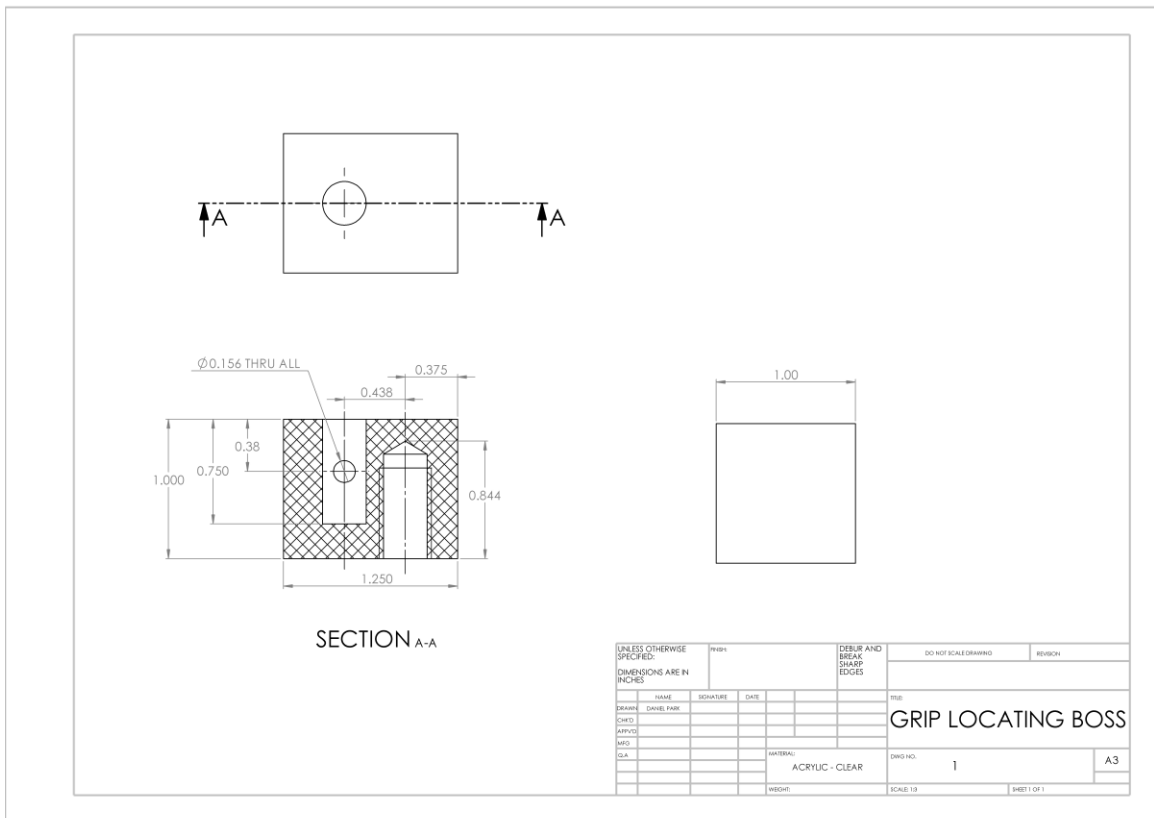
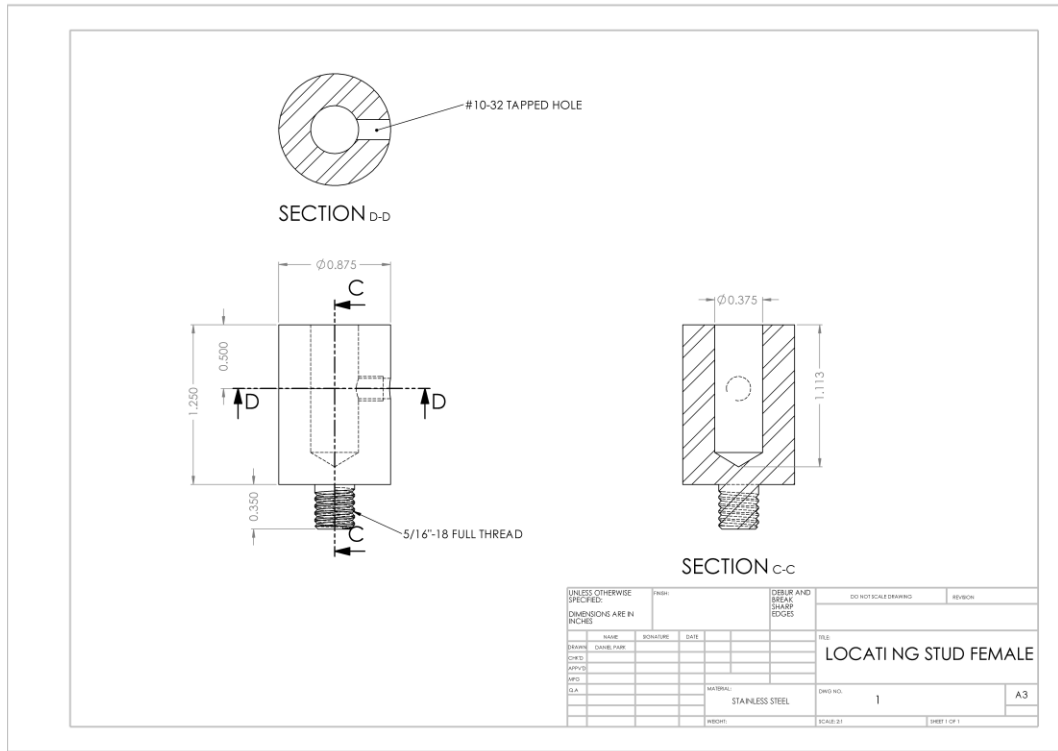


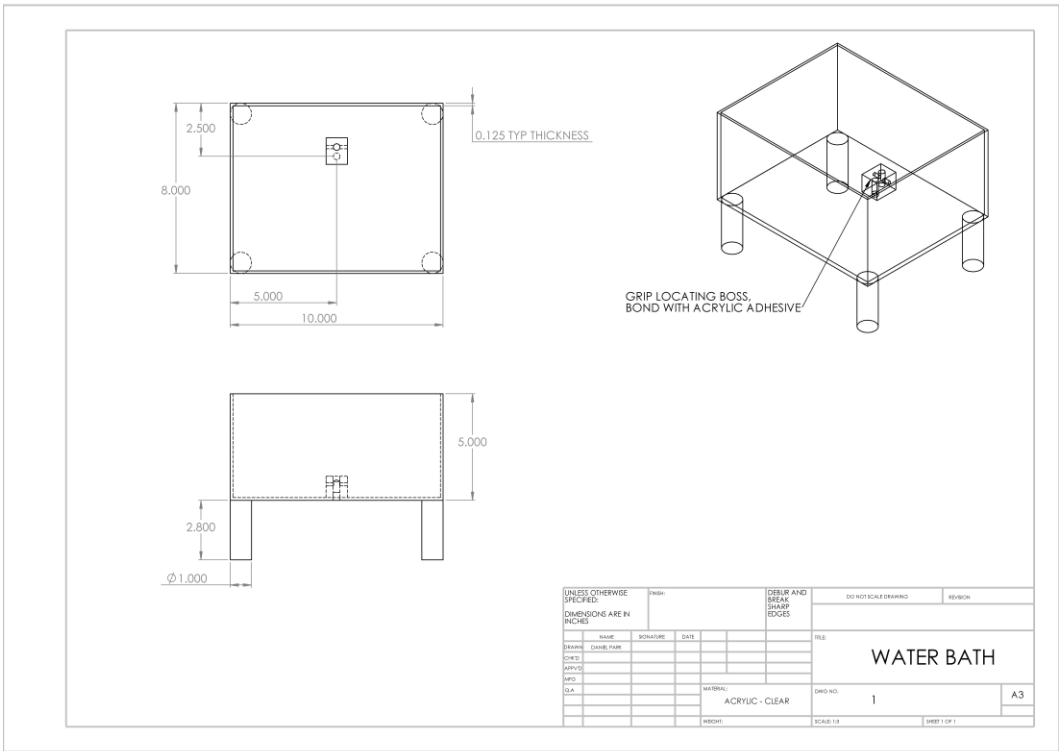
The above results are ultimate extension (%) of ring shaped samples cut from cast tubular 10 w% PVA samples, freeze-thaw cycles n=1-6. Methods of calculation as well as diagrams of ring extension grips can be found in the standard. Standard tensile grips tend to slip before fracture in the soft tissue grips, ring samples were used to test ultimate extension of hydrogel samples.

Appendix B: Tensile Fixture Drawings









UNLESS OTHERWISE SPECIFIED: DIMENSIONS ARE IN INCHES		FINISH	DRAW AND BREAK SHARP EDGES		DO NOT SCALE DRAWING	REVISION
NAME	SIGNATURE	DATE	TITLE			
DESIGNED	DATE PAID		WATER BATH			
CHECKED						
APPROVED						
DATE						
MATERIAL: ACRYLIC - CLEAR			DRAWING NO. 1	A3		
REVISION			SCALE: 1:1	SHEET 1 OF 1		

Appendix C: ASCII command table for ESM301L test stand

5.8 PC Mode

The ESM301 can be controlled by a PC via serial communication. A list of supported ASCII commands is provided below:

Command	Description	Example
a	Request speed	
b	Set travel units to inches	
c	Enter cycle mode	
d	Move crosshead down	
e	Set speed	
	Inch format: eXX.XX Two leading zeroes and two decimal places required.	e02.85 = 2.85 in/min
	Millimeter format: eXXXX.X Four leading zeroes and one decimal place required.	e0200.3 = 200.3 mm/min
f	Set cycles. Format: fXXXX (leading zeroes required)	f0500 = 500 cycles
g	Set lower travel limit	
	Inch format: g-XX.XXX Negative sign (if applicable), two leading zeroes, and three decimal places required.	g-00.550 = -0.55 in g01.258 = 1.258 in
	Millimeter format: g-XXX.XX Negative sign (if applicable), three leading zeroes, and two decimal places required.	g-007.52 = -7.52 mm g010.70 = 10.7 mm
h	Set upper travel limit	
	Inch format: h-XX.XXX Negative sign (if applicable), two leading zeroes, and three decimal places required.	h-00.550 = -0.55 in h01.258 = 1.258 in
	Millimeter format: h-XXX.XX Negative sign (if applicable), three leading zeroes, and two decimal places required.	h-007.52 = -7.52 mm h010.70 = 10.7 mm
i	Set travel units to millimeters	

Model ESM301 / ESM301L Test Stand

User's Guide

j	Set crosshead speed to maximum speed	
k	Set crosshead speed to minimum speed	
l	Enter travel limit mode	
m	Enter manual mode	
n	Transmit travel and force readings	
o	Set crosshead speed to programmed speed	
p	Request stand status*	
q	Request number of cycles completed	
r	Request number of cycles set	
s	Stop crosshead	
t	Reset cycle counter to zero	
u	Move crosshead up	
v	Request upper travel limit	
w	Request lower travel limit	
x	Request travel value	
z	Reset travel to zero	

* The transmission of ASCII "p" will return the stand status. The following are the return codes and their definitions:

	Command	Description
Crosshead status	U	Crosshead moving up
	D	Crosshead moving down
	S	Crosshead stopped
Operating mode	C	Cycle mode
	L	Limit mode
	M	Manual mode
Limit switch status	UL	Crosshead at upper limit
	DL	Crosshead at lower limit

Curriculum Vitae

Name: Daniel James Park

**Post-secondary
Education and
Degrees:**

University of Western Ontario
London, Ontario, Canada
2008-2013 B.E.Sc. Mechanical Engineering

**Related Work
Experience:**

- Internship – Lifelike BioTissue (2011-12)
- Graduate Teaching Assistant – Western University (2014-15)

**Conference
Publications:**

D.J. Park, A.N. Hrymak, L.E. Millon, “Polymer Systems and Molding Techniques for General Surgery Training Models” *30th International Conference of the Polymer Processing Society*, June 8-12, Cleveland, Poster Presentation (2014)